https://doi.org/10.5194/hess-2022-48
Preprint. Discussion started: 8 February 2022

Hydrology and Earth System Sciences
Discussions

Studying the dynamic of a high alpine catchment based on multiple natural tracers

Anthony Michelon[1], Natalie Ceperley[2], Harsh Beria[3], Joshua Larsen[4], Torsten Vennemann[1], Bettina Schaefli[1,2]

[1]Institute of Earth Surface Dynamic (IDYST), Faculty of Geosciences and Environment (FGSE), University of Lausanne, Lausanne, Switzerland
[2]Institute of Geography (GIUB) and Oeschger Center of Climate Change Research (OCCR), University of Bern, Bern, Switzerland. Bettina Schaefli: Institute of Geography
[3]Department of Environmental Systems Science, ETH Zurich, Zurich, Switzerland
[4]School of Geography, Earth and Environmental Sciences, University of Birmingham, Birmingham, UK

Correspondence to: Bettina Schaefli (bettina.schaefli@giub.unibe.ch)

Abstract.

Hydrological processes in high elevation catchments are largely influenced by snow accumulation and melt, as well as summer rainfall input. The use of the stable isotopes of water as a natural tracer has become popular over recent years to characterize water flow paths and storage in such environments, in conjunction with electric conductivity (EC) and water temperature measurements. In this work, we analyzed in detail the potential of year round samples of these natural tracers to characterize hydrological processes in a snow-dominated Alpine catchment. Our results underline that water temperature measurements in springs, groundwater and in-stream are promising to trace flow path depth and relative flow rates. The stable isotopes of water are shown here to be particularly valuable to get insights into the interplay of subsurface flow and direct snowmelt input to the stream during winter and early snow melt periods. Our results underline the critical role of subsurface flow during all melt periods and the presence of snowmelt even during winter base flow. We furthermore discuss why reliably detecting the role of subsurface flow requires year-round water sampling in such environments. A key conclusion of our work is the added value of soil and water temperature measurements to interpret EC and isotope analyses, by giving additional information on snow-free periods and on flow path depths.

1 Introduction

Hydrology in Alpine environments is largely dominated by snow accumulation and melt processes compared to summer rainfall, with ensuing high sensitivity to changes in climate (Hanus et al., 2021). For Alpine catchments with a mean elevation above approximately 1,500 masl (Santos et al., 2018), winter snowfall leads to the build-up of a seasonal snowpack, which in the northern hemisphere results in low flow occurring between November and March (Schaefli et al., 2013) and maximum monthly streamflow related to melt between May and August, depending on the depth and extent of the seasonal snowpack

https://doi.org/10.5194/hess-2022-48
Preprint. Discussion started: 8 February 2022


Hydrology and Earth System Sciences
Discussions

and on the degree of glacier cover (Hanus et al., 2021; Muelchi et al., 2021). Given the importance of these cycles of accumulation and melt and the resulting streamflow regime for water resources availability, an important body of literature focuses on quantifying the streamflow regime in such environments, either based on streamflow observations (Blahusiakova et al., 2020; Brunner et al., 2019; Musselman et al.; Hammond and Kampf, 2020) or modelling (Foster et al., 2016; Livneh and Badger, 2020; Muelchi et al., 2020).

Detailed hydrological process studies in high Alpine catchments remain, however, relatively rare even if detailed insights into the fate of rainfall and snowmelt in such catchments are required for model-based extrapolations of their hydrological response into the future, given the likely changes in climate. In addition to logistical challenges, the difficulties to access and continuously monitor in temporally frozen environments requires the development of specific methods and equipment (Rucker et al., 2019), which is certainly one of the main reasons to explain the small number of studies in such places.

Existing field-based studies can be classified according to their focus: i) understanding dominant runoff generation mechanisms during rainfall and snowmelt events (Penna et al., 2016; Engel et al., 2016), including small-scale studies of snowpack flow paths (Webb et al., 2020), ii) understanding the origin of winter low flow (Floriancic et al., 2018), iii) quantification of groundwater or spring recharge (Lucianetti et al., 2020) and seasonal groundwater storage (Arnoux et al., 2020) or iv) understanding the role of glaciers and rock-glaciers in the hydrological response of high elevation catchments (Brighenti et al., 2019; Zuecco et al., 2019; Ohlanders et al., 2013; Penna et al., 2014). A common feature of these studies is the use of natural tracers, such as electric conductivity and/or stable isotope composition of water, for example, to gain new insights into the fate of rainfall and snowfall and related water flow paths and to formulate hypotheses about dominant runoff drivers at specific times of the year, or about the hydrologic response of selected landscape units.

To complement such existing studies, this work attempts to quantify dominant drivers of the hydrologic response of a high elevation catchment throughout the year, i.e. through all streamflow periods, ranging from winter low flow, to different stages of the melt season and the autumn recession. We analyze the observational data from the intensively studied Vallon de Nant catchment in the Swiss Alps (Benoit et al., 2018; Giaccone et al., 2019; Ceperley et al., 2020; Mächler et al., 2021; Michelon et al., 2021a; Thornton et al., 2021a; Beria et al., In revision; Antoniazza et al., Submitted).

This work focuses on what we can learn about water flow paths from stable isotope composition of water, a natural tracer that has been extensively used to characterize hydrological processes related to snow (e.g. Beria et al., 2018). The analysis of stable isotope compositions of water can give insights into different water sources (such as rainfall, snowpack, springs, groundwater), recharge and evaporation processes (e.g. Sprenger et al., 2016); it is complemented here by electrical conductivity measurements that provide additional information on subsurface flow paths and relative water residence times in the subsurface (Cano-Paoli et al., 2019), by temperature measurements of water to trace connectivity between water sources and the atmosphere (Constantz, 2008), and by soil temperature measurements to gain insights into periods of thermal insulation from the seasonal snowcover (Trask et al., 2020).

The specific objective of this work is to examine the dominant hydrological processes that explain the catchment-scale hydrological response during different periods of the year. Key open questions include the origin of winter streamflow (from

https://doi.org/10.5194/hess-2022-48
Preprint. Discussion started: 8 February 2022


Hydrology and Earth System Sciences
Discussions

subsurface storage versus from localized snow melting) (Floriancic et al., 2018; Hayashi, 2020), the dominant runoff processes that drive streamflow generation during early spring snow melt (Brauchli et al., 2017) and later on in the snowmelt season and the role of shallow groundwater in the hillslopes and of alluvial or talus groundwater systems (Hayashi, 2020) in the streamflow generation throughout the year. In addition, the aim is to provide transferable insights into the value of the observed variables for hydrologic process investigations in comparable catchments.

2 Case study

2.1 Study area

The following case study description is largely based on the paper by Michelon et al. (2021a). The Vallon de Nant is a 13.4 km² headwater catchment located in the western Swiss Alps (Figure 1) and has an elevation range from 1,200 to 3,051 masl (mean 2,012 masl). The catchment has an elongated shape and runs from south to north. The main stream is the Avançon de Nant.

The area is of national importance in Switzerland for its biodiversity (Cherix and Vittoz, 2009) and is protected since 1969 (Natural Reserve of the Muveran). The Vallon de Nant has been the focus of a number of recent research projects, in disciplines such as hydrology (Michelon et al., 2021a; Beria et al., 2020), hydrogeology (Thornton et al., 2021a), pedology (Rowley et al., 2018) biogeochemical cycling (Grand et al., 2016), geomorphology (Lane et al., 2016) and vegetation ecology (Vittoz, 2012; Giaccone et al., 2019), as well as interaction between biology and hydrology (Mächler et al., 2021) and stream ecology (Horgby et al., 2019).

The catchment belongs to the backside of the Morcles nappe (Huggenberger, 1985). The Cretaceous and Tertiary lithologies are organized as a succession of thick, blocky layers exposed throughout the surrounding valley. They lie on a substratum of flysch, i.e. softer rocks (schistose marls and sandstone benches), which explains the deepening and widening of the valley at its southern part (Badoux, 1991).

In the southern part of the valley the Glacier des Martinets, with a surface of 0.58 km² in 2016 (Linsbauer et al., 2021) survives at relatively low elevation (2,126 to 2,685 masl) as it lies on the northern, shady side of the Dent de Morcles. Due to its small size, its high debris cover and low radiation exposure, the glacier is likely to have a small contribution to the catchment-scale streamflow (Mächler et al., 2021). The water flow paths through and below the debris-covered glacier are unknown to date and are not specifically investigated as part of the present research.

The eastern side of the catchment is marked by steep and rocky slopes associated with shallow soils and debris cones at the foot of the rock walls in the north-eastern part. Along the rock walls, all lateral tributaries are ephemeral, flowing principally during the snowmelt season or shortly after the rainfall events; their extent fluctuates and is not known precisely.

The western side of the valley is associated with grassy slopes, relatively well-developed soils and hence relatively high water storage capacities; the latter also indicated by salt gauging along the main stream during the late summer and autumn streamflow recession period in 2016 and 2017 (see Figure S5 in Supplementary Material).

https://doi.org/10.5194/hess-2022-48
Preprint. Discussion started: 8 February 2022


Hydrology and Earth System Sciences
Discussions

The location of springs seems correlated with low slopes (see Figure S6 in Supplementary material) and this topographic particularity might be enough to explain the location of springs along the right bank of the main stream and within the grassy slopes in the west area of the catchment, where the slopes are low. In the same way, the absence of tributaries over the north-western parts of the catchment can be related to steep slopes but can also be explained by a large hydraulic conductivity and locally well-developed soils.

The riparian wetland (Figure 1), at least in its southern part, is made of coarse and permeable alluvial sediments associated with a high hydraulic conductivity; it could be "hydrologically active" to its full depth, which can exceed 80 m (Thornton, 2021).

The extent of the stream network is based on observations during dry and wet periods (Michelon et al., 2021a) and its exact path is calculated using the Swiss digital elevation model at a resolution of 2 m (swissAlti3D, 2012). During wet periods, the stream network (as shown in Figure 1) has a maximum length of around 6 km; during dry periods outside the melting season and before the snow accumulation period, the main stream can be as short as 2.95 km, corresponding to a start of channelized flow at 1480 masl. During the snow accumulation season, the stream network extent is difficult to establish but the river never falls dry at the outlet (i.e. no known occurrence of zero flow).

A comparison of historical and recent photographs (see Figure S2 in Supplementary Material) shows a relatively stable vegetation cover, composed of grassland and spruce. The distribution of stands of spruce (Dutoit, 1983), which are intermixed with corridors of scrub vegetation on the north-western slopes, are controlled by regular avalanches.

https://doi.org/10.5194/hess-2022-48
Preprint. Discussion started: 8 February 2022

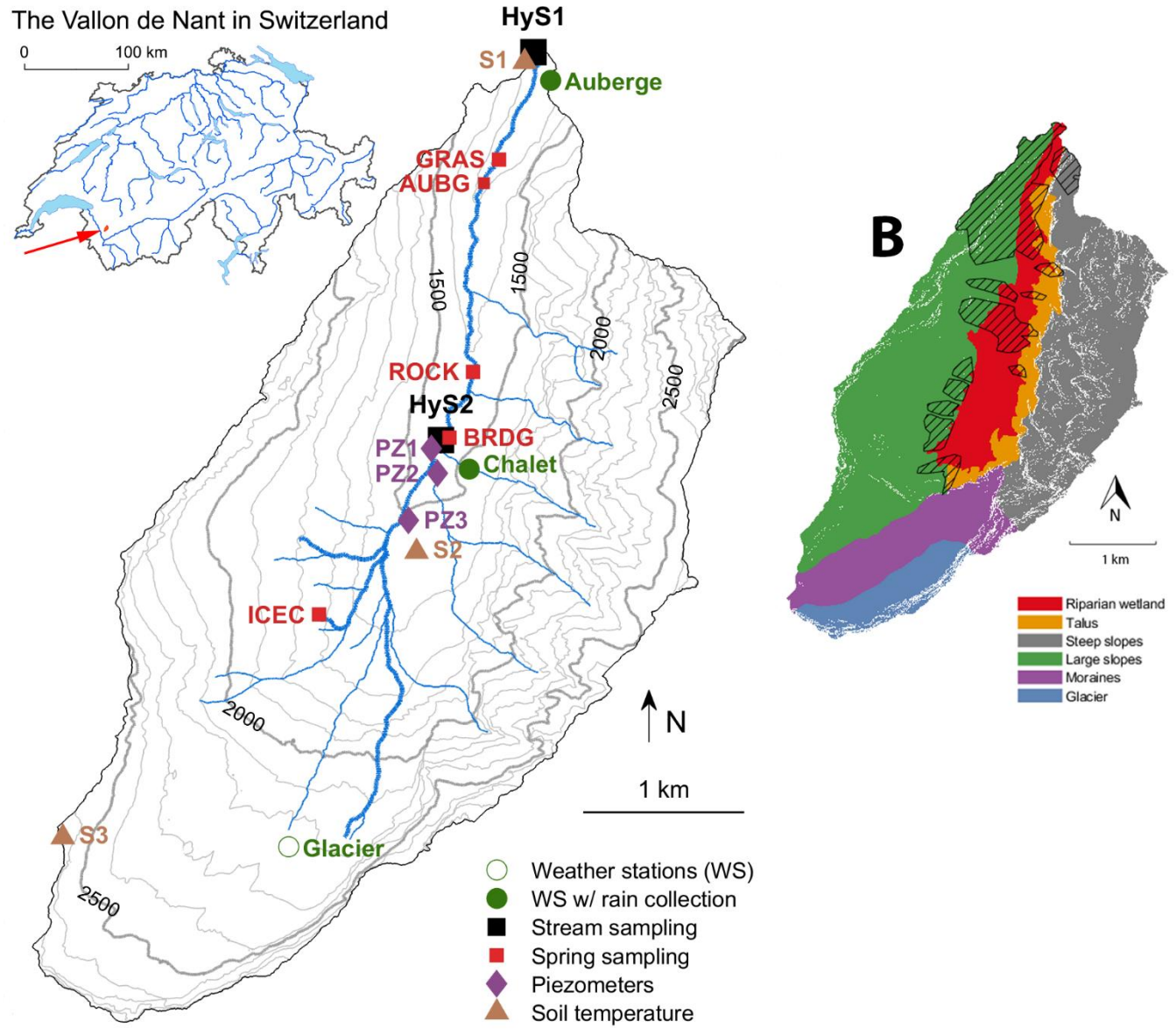

Figure 1. The map A) shows the location of the sampling sites in the Vallon de Nant (outlet at 46.25301°N, 7.10954°E in WGS84). Note that the AUBG spring location shows where the spring is picked up, whereas the water from this spring is sampled at the Auberge weather station point, 800 m further north. The topographic map is based on a digital elevation model at a resolution of 2 m (swissAlti3D, 2012). The stream network shows its full extend during snowmelt periods. 'Soil temperature' shows locations of the sensor network of Vittoz (2021). The map B) identifies the dominant hydrological units of the Vallon de Nant and the hatched area corresponds to forested areas.

https://doi.org/10.5194/hess-2022-48
Preprint. Discussion started: 8 February 2022


Hydrology and Earth System Sciences
Discussions

2.2 Meteorological and hydrological characterization of the study period

The streamflow at the outlet is monitored since September 2015 via river height measurements using an optical height gauge (VEGAPULS WL-61 optical height gauge, VEGA, Schiltach, Germany) above the middle point of a trapezoid shape weir. It averages water height every minute continuously. The height is then converted into streamflow using a rating curve based on 55 salt streamflow measurements (Ceperley et al., 2018). We fit a power-relationship using the nonlinear least squares fitting algorithm of MathWorks MatLab's "fit" function (The MathWorks, 2017) with the trust region algorithm and least absolute residual method to obtain a 95% confidence interval.

The annual average streamflow calculated over 2017 and 2019 is between 0.46 to 0.62 $m^3 s^{-1}$ (3.0 to 4.0 mm d^{-1}) but fluctuates between 0.02 to 0.03 $m^3 s^{-1}$ (0.12 to 0.18 mm d^{-1}) and 2.4 to 3.1 $m^3 s^{-1}$ (15.5 to 19.7 mm d^{-1}). Flood events can cause streamflow from 5.8 to 7.2 $m^3 s^{-1}$ (37.4 to 46.3 mm d^{-1}) over 1 hour and from 6.9 to 8.5 $m^3 s^{-1}$ (44.4 to 54.6 mm d^{-1}) over 10 minutes. The mean temperature of the streamflow at the outlet is 5.0 °C, ranging from 0 °C when the river is frozen during some winter periods to a daily temperature of 10.0 °C during summer.

The Avançon de Nant river shows a typical snow dominated streamflow regime with a high flow period during spring and early summer (Figure 2) when the catchment releases water due to accumulation and melt of the seasonal snowcover. During the study period, peak monthly flow was either in June (for 2017-2018 and 2018-2019) or July (2016-2017 with a snow rich winter).

Meteorological variables are monitored at three locations (Michelon et al., 2021b) along a north/south transect (at 1253 masl, 1530 masl and 2136 masl) since September 2016. The precipitation intensity is measured using a 24 GHz Doppler radar sensor (Lufft WS400-UMB, G. Lufft Mess- und Regeltechnik GmbH, Fellbach, Switzerland) that distinguishes the precipitation phase (rain and snow). From these 3 stations, the annual mean air temperature at mean elevation (2,012 masl) is estimated to 3.1 °C in 2017.

https://doi.org/10.5194/hess-2022-48
Preprint. Discussion started: 8 February 2022

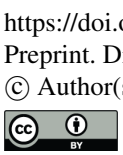

Hydrology and Earth System Sciences
Discussions

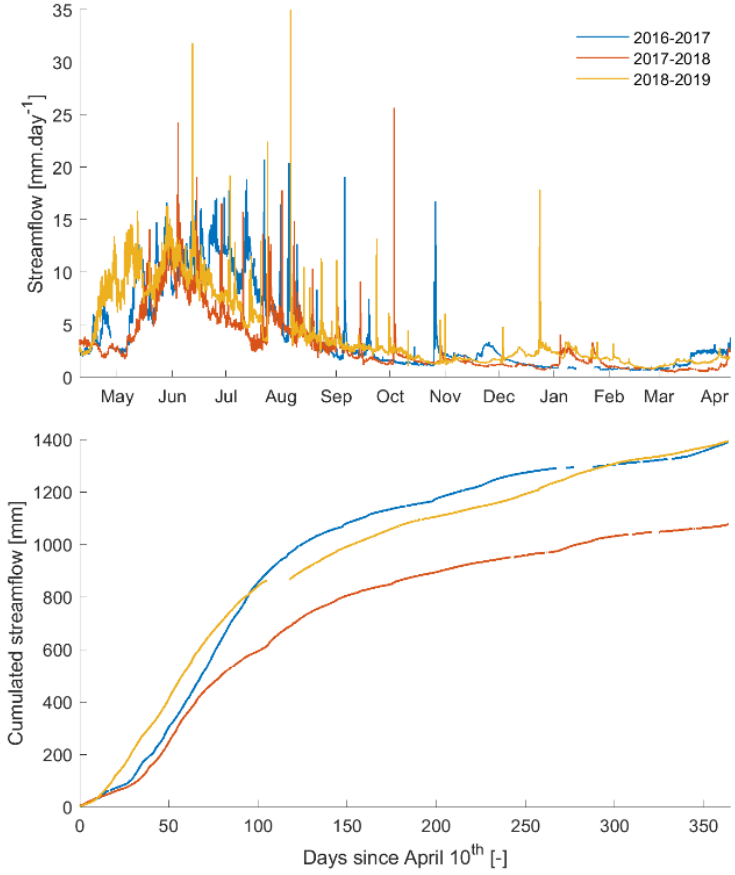

145 Figure 2. Comparison of the streamflow evolution (on top) and cumulative (bottom) over a year (April 10th to April 9th next year) for 3 years. Note that there are gaps in the data, and 6.4%, 3.2% and 4.6% of the timeseries are missing (respectively in 2016-2017, 2017-2018 and 2018-2019).

3 Method

Below, we describe the hydrological process monitoring equipment and sampling methods deployed during the study period
150 (from 2016 to 2018).

3.1 Stable isotopes of water

3.1.1 Water sampling

Water was either sampled manually (grab samples) or via automatic samplers placed at the outlet and an upstream location along the stream (HyS1 and HyS2, see Figure 1) for stable isotope analysis (δ^2H, $\delta^{17}O$ and $\delta^{18}O$). Manual samples were
155 collected from streams, springs and piezometers using 12 mL amber borosilicate glass vials with polypropylene screw-top caps with PTFE-lined silicone septa. Automatic sampling was performed with an ISCO 6712C Compact Portable Sampler

https://doi.org/10.5194/hess-2022-48
Preprint. Discussion started: 8 February 2022


Hydrology and Earth System Sciences
Discussions

with 24 bottles of 500 mL capacity at HyS1 and an ISCO 6712 full-size portable sampler with 24 bottles of 1L capacity at HyS2 (Lincoln, Nebraska, USA). Automatic samplers were programmed to sample at 6 hours intervals over one week. The automatic sampler was programmed to fill bottles to half of their capacity, 250 mL and 500 mL, respectively, to optimize energy usage and to prevent sample loss due to freezing, while still sampling enough water such to keep fractionation due to evaporation would be insignificant.

A sub-sample of water was then taken manually from each bottle using a 12 mL amber glass vial (either in the laboratory or in the field). Original installation involved the use of pipettes and tubes inside the autosampler bottles similar to those described by von Freyberg et al. (2020), however after some experimentation and due to the alpine and shaded microclimate of the location, fractionation due to evaporation was deemed minimal and additional components resulted in more contamination and less sampling capacity. In case of freezing, the bottles were closed with a cap and moved to a warmer place until the ice fully melted. The same borosilicate glass vials were also used for long-term storage at ambient temperature in the laboratory.

Samples of rainfall were collected at the *Auberge* and *Chalet* meteorological stations (Figure 1) with a 13 cm of diameter plastic funnel, connected to an insulated 2.5 L screw-top bag made of 147 µm PET/NY/LDPE plastic (DaklaPack, Perpignan, France), enclosed in a plastic box. The collected water was well mixed, weighed and sub-sampled using 12 mL amber glass vial once or twice a week from May to November (i.e. outside the snowfall period).

Groundwater was sampled from piezometers installed for a simultaneous hydrogeological study (Thornton et al., 2021a). Prior to water sampling, the piezometers were emptied using a Geotech Peristaltic Pump (Geotech Environmental Equipment, Inc, Denver, Colorado, U.S.A.); and the freshly recharged water was sampled with the same pump and stored in 12 mL amber glass vials.

During winter 2017 and winter 2018, snow samples were collected regularly at two locations. Two different sampling methods were used: i) if distinguishable snow layers were present (visual and textural distinction) each of them was sampled individually, otherwise ii) a single bulk sample of approximately sampled the entire profile was taken.

Snow samples were sealed in alimentary 700 mL zip bags made of 120 µm BOPP/LPDE plastic (DaklaPack, Perpignan, France) after evacuating as much air as possible. The collected snow samples were melted at ambient air temperature (the influence of water vapor from air on the isotopic composition of the sample is discussed in the Appendix 1). A sub-sample of well-mixed, melted snow was taken manually in the lab from each bag into a 12 mL amber glass vial.

The isotopic composition of the entire snowpack at a given snow pit was obtained with a weighted average of the values of each sampled layer according to depth, as an approximation for the equivalent bulk isotope composition assuming a uniform density.

For vegetation, the isotopic ratio of water is extracted cryogenically from xylem and near-by surface soil collected from two transects of 10 *Larix decidua* individual trees running about 200 m perpendicular to the main stream just below and above 1500 masl during the 2017 and 2018 growing season (Ba, 2019).

https://doi.org/10.5194/hess-2022-48
Preprint. Discussion started: 8 February 2022


Hydrology and Earth System Sciences
Discussions

3.1.2 Analysis of the isotopic composition of water

Stable isotope composition of water, expressed as the familiar δ^2H, $\delta^{17}O$ and $\delta^{18}O$ notation, were analyzed with a Picarro 2140-i Wavelength-Scanned Cavity Ring Down Spectrometer (Picarro Inc., Santa Clara, California, U.S.A.), using 2.0 mL glass vials closed with screw-top caps with silicone Rubber/TPFE septa filled with 1.8 mL of filtered water. Samples were injected between 6 and 8 times. The first 3 injections were discarded to avoid memory effects. The raw values were then corrected according to a standard curve determined with 3 internal standards, which are regularly calibrated against the international standards of VSMOW (Vienna Standard Mean Ocean Water) and SLAP (Standard Light Antarctic Precipitation) of the IAEA (International Atomic Energy Agency)(Coplen, 1994). Each standard was injected 12 to 15 times, and the last 6 injections were kept. Delta units of isotope compositions (Coplen, 1994) are reported in per mil and the strategy used for the analysis is similar to the one described in the work of Schauer et al. (2016). The median analytical errors obtained with this method are 0.4 ‰ for δ^2H, 0.01 ‰ for $\delta^{17}O$, 0.04 ‰ for $\delta^{18}O$.

Based on these measures, we compute d-excess (Dansgaard, 1964) and ^{17}O-excess (Barkan and Luz, 2005; Landais et al., 2006):

$$\text{d-excess} = \delta^2H - 8 \cdot \delta^{18}O, \quad (1)$$

$$^{17}\text{O-excess} = 10^6 \left(ln\left(\frac{\delta^{17}O}{1000} + 1\right) - \lambda_{ref} \cdot ln\left(\frac{\delta^{18}O}{1000} + 1\right)\right). \quad (2)$$

With λ_{ref} = 0.528 (Meijer and Li, 1998; Barkan and Luz, 2005; Landais et al., 2008). From regression of $\ln(\delta^{17}O/1000 + 1)$ against $\ln(\delta^{18}O/1000 + 1)$, we obtain a similar slope for our samples (λ_{ref} = 0.528), which confirms the universality of this value.

The d-excess and ^{17}O-excess aretypically used to investigate the large scale hydrological cycle and oceanic moisture sources (Nyamgerel et al., 2021). Both d-excess and ^{17}O-excess are known to be sensitive to relative humidity during evaporative processes but ^{17}O-excess is supposed to be less temperature sensitive (Surma et al., 2021; Bershaw et al., 2020) than d-excess and can thereby convey additional information on evaporation processes and on climatic conditions (Risi et al., 2010).

To gain insights into local evaporative processes, we compute the line-conditioned excess lc-excess (Landwehr and Coplen, 2006) based on our local meteoric water line LMWL ($\delta^2H = a \cdot \delta^{18}O + b$), which significantly deviates from the global meteoric water line GMWL (see Section 4.5).

$$\text{lc-excess} = \delta^2H - a \cdot \delta^{18}O - b. \quad (3)$$

The LMWL is calculated using linear regression between $\delta^{18}O$ and δ^2H of 85 rainfall samples and yields coefficients a=7.38 and b=6.15.

The median analytical error is 0.4 ‰ for d-excess and lc-excess, and 8 per meg for ^{17}O-excess.

https://doi.org/10.5194/hess-2022-48
Preprint. Discussion started: 8 February 2022


Hydrology and Earth System Sciences
Discussions

3.2 Water temperature and conductivity measures

The water temperature of four springs was recorded every 30 minutes (every 15 minutes for GRAS and ROCK springs) with Hobo temperature loggers (Onset Computer Corporation, Bourne, MA, U.S.A.) for periods between 12 and 21 months. Based on these recordings, we estimate lag times with respect to air temperature and diel and annual amplitudes. The original time resolution of 1 minute for the stream, 30 minutes for piezometers (PZ) and 2 minutes for springs is kept for the diel temperature maximum amplitude but aggregated to 1 day for the annual temperature maximum amplitude (using a 7-day moving average). Lag times are obtained by maximizing cross correlation between the 1-day signal and the one for the reference air temperature signal (at Auberge station). Electrical conductivity (EC) was measured for all collected water samples except snowpack, either directly in the field with a WTW Multi 3510 IDS connected to a WTW TetraCon 925 probe (Xylem Analytics Germany Sales GmbH & Co, Weilheim, Germany) or in the laboratory directly in the 12 mL amber silicate vials using a JENWAY 4510 Conductivity Meter with a 6 mm glass probe (Stone, U.K.). Comparison of duplicate measurements using both probes (compensated in temperature) demonstrated a correlation coefficient of R^2=0.89 despite a delay of 23 to 30 months between the in situ and laboratory measurements (see Figure S7 in Supplementary Material).

3.3 Additional data sources

Our own data set is complemented by data obtained from an existing sensor network to measure soil temperature (see Figure 1), which was deployed in the context of vegetation research (Vittoz, 2021) and recorded hourly soil temperatures at four locations from July 2009 to November 2018 using GeoPrecision M-Log5W (GeoPrecision GmbH, Ettlingen, Germany) buried at 10 cm depth. The soil temperature can be assumed to be a good proxy for snow cover, making distributed data throughout the catchment area particularly useful to us. Strong diel variations of soil temperature (measured at 10 cm) can in fact be associated with snow-free soils, which are typically exposed to large amplitude air temperature fluctuations and radiative exchanges.

Piezometric data originally collected as part of the work of Thorton et al., (2021) from two locations in the alluvial flood plain (Figure 1) allowed us to characterize the corresponding ground water system.

We obtained a long air temperature time series from a grided product (1 x 1 km grid) from MeteoSwiss (MeteoSwiss, 2019). The gridded data is influenced by of the low number of stations at high elevations (Freudiger et al., 2016) but compared to our own meteorological data, the gridded temperature times series shows a satisfactory level of correlation at a daily scale ($0.96 < R^2 < 0.98$), and is thus useful for gap filling.

https://doi.org/10.5194/hess-2022-48
Preprint. Discussion started: 8 February 2022


Hydrology and Earth System Sciences
Discussions

4 Results

4.1 Identification of streamflow periods

To guide the analysis of what might explain the streamflow response during different times of the year, the hydrograph was divided into a series of periods, after smoothing to original 1-min recordings with a 7-day moving average. The retained periods are called baseflow period (B), early melt period (E), melt period (M) and seasonal recession period (R); they are illustrated in Figure 3 along with the hydrograph. The baseflow period extends from the end of September to early spring (mid-March to beginning of April) and shows a streamflow of around 1 mm/d only, which is typical for catchments at comparable elevations (Floriancic et al., 2018). The baseflow exhibits a very slow streamflow decrease throughout the period and almost no diel variations even though some streamflow peaks might occur due to exceptional rainfall events or warm periods (e.g. January 2018). During the early melt period, the streamflow starts increasing to a few mm/d, preceding the main snow melt period. This early melt period lasts several weeks in certain years (e.g. in 2017), with an increase in streamflow to around 3 mm/d, followed by a plateau that lasts approximately 49 days. In 2018, warming occurred extremely quickly, thus no early melt period existed (Figure 3). This early melt period is rarely explicitly discussed in the literature (for a model-based example, see He et al., 2015), despite the fact that it is a typical pattern and remains challenging to model (see Figure 9 in Brauchli et al., 2017; or Figure 3 in Thornton et al., 2021b).

The melt period is characterized by an increase of the streamflow due to an important water input from snowmelt. Over the course of our observation period, the melt period started at the beginning of May in 2017, and at least a month earlier in 2018 (though this was the year without a clearly visible early melt period). The annual 7-day streamflow maximum marks the start of the seasonal recession period, which for 2017 and 2018 corresponds to the end of May or beginning of June, but only to the end of June in 2016, which was preceded by a very snow-rich winter. The seasonal recession results from a combination of reduced input from snowmelt and evaporation.

4.2 Soil temperature

4.2.1 Temporal patterns

The soil temperature data from three different elevations (at 1240 m, 1530 m, and 2640 masl, see Figure 1) shows how the insulation provided by the snow cover dampens the high frequency (diel) air temperature variations (positives and negatives, see Figure 3). Before the start of each winter period, the soil temperature approaches gradually 0 °C, with only a slightly positive temperature that is caused by heat flux from the ground. However, some isolated temperature spikes are observed during winter, most probably due to rain-on-snow events (e.g. the spike during winter 2016 in the green line in Figure 3, representing the lowest elevation). Unfortunately, no other observed tracers are available during these periods to confirm this hypothesis.

The negative temperatures measured during the 2016-2017 winter period by two soil temperature probes (at 1530 m and 2640 masl) are reached due to cold air temperatures associated with an exceptionally dry winter and low snow cover.

https://doi.org/10.5194/hess-2022-48
Preprint. Discussion started: 8 February 2022


Hydrology and Earth System Sciences
Discussions

The temperature recordings at the three different elevations in Figure 3 show the start of the snow-free period at each measurement location with a sharp warming between March and July (depending on elevation) of more than 5 °C. The start of the snow-free period shows a delay of between 4 (2018) and 8 weeks (2017) between the elevation 1240 m and 1530 masl Comparing the elevation 1530 m to 2640 masl, the start of the snow free period is delayed by 3.5 (2018) and 8 weeks (2016). Similarly, the soil temperature time series clearly show the much earlier seasonal snow cover onset in autumn 2016 at the highest elevation as compared to the two lower elevations (12 weeks earlier). In 2017, the seasonal snow cover onset occurred at a similar time at all elevations, visible as a stop of all diel temperature variations, between October 22nd and November 25th, 2017). A summary of snow-free dates as extracted from the temperature recordings is available in the Supplementary Material (Table S2).

Finally, it is noteworthy that, albeit not the focus of this paper, the soil temperature recordings and their co-variation with streamflow show that during summer, rainfall input coincides with cold spells; during autumn, rainfall input coincides with warm spells (e.g. October 2016 and 2017).

https://doi.org/10.5194/hess-2022-48
Preprint. Discussion started: 8 February 2022

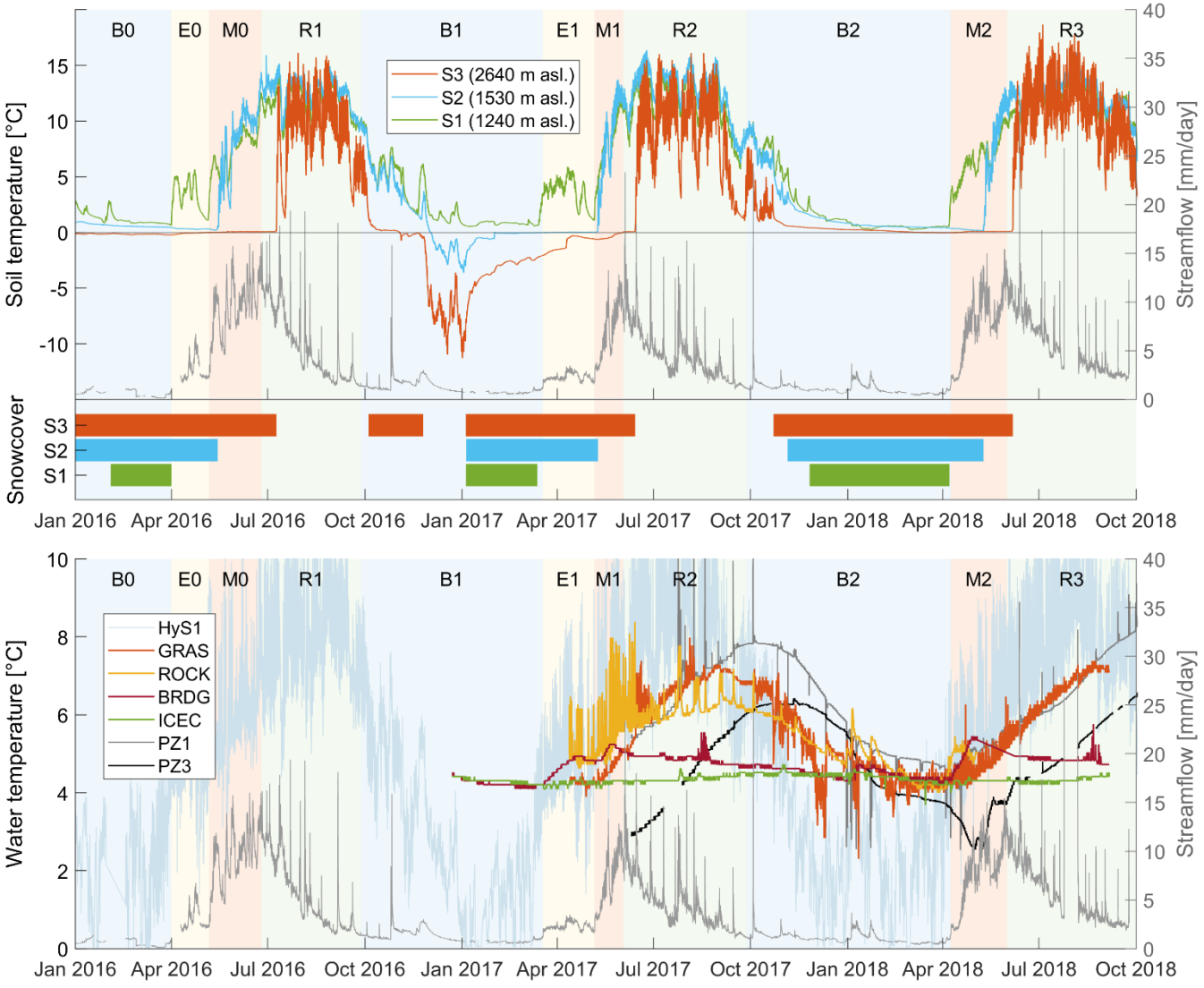

290 Figure 3. Evolution of soil temperature (top) at 3 locations within the Vallon de Nant catchment and (bottom) of the stream at the outlet, 4 springs and groundwater at 2 locations between January 2016 and October 2018. A summary of dates is available in the Supplementary Material (Table S1).

4.2.2 Link to streamflow

The soil temperature measurements reveal interesting features with respect to the identified streamflow periods. For all three
295 summers, the soil temperature recordings from the highest elevation show the presence of snow until the start of the recession period, which underscores the late melt of seasonal snow in some areas of the catchment. The start of the two early melt-dominated streamflow periods in 2016 and 2017 corresponds to the disappearance of snow at the lowest soil temperature measurement point. This suggests that this early melt streamflow rise might well be linked to locally complete snow melt and

https://doi.org/10.5194/hess-2022-48
Preprint. Discussion started: 8 February 2022


Hydrology and Earth System Sciences
Discussions

associated water input to the stream at the lowest elevations, during periods when higher up, any potential snow melt is still being retained in the existing snow pack or subsurface.

Soil temperature recession starts at a similar date at all elevations and is in close correspondence with the start of the streamflow baseflow periods; i.e. significant decrease of soil temperature only starts when the streamflow recession period is already well advanced. In the winter of 2016/2017, winter streamflow fluctuations are reflected in the soil temperature, whereas the mid-winter streamflow rise in January 2018 is not visible in any of the soil temperature recordings, which may be due to errors in recording river stage caused e.g. by accumulated sediments.

4.3 Water temperature

4.3.1 Influence of air temperature on stream temperature

Average recorded stream temperature at the outlet corresponds to 5.0 °C, which is slightly higher than the average recorded air temperature at mean elevation 2,012 m asl, which equals 3.1 °C. The fluctuations of the water temperature at the catchment outlet (HyS1, Figure 1) are correlated with the variations of the air temperature (R^2 = 0.87 between water temperature and air temperature at the Auberge weather station) and the annual cycle shows no lag with respect to air temperature. This can be explained by the fact that the in-stream travel time is long enough for atmospheric heat exchange to exert a strong influence on water temperatures (Gallice et al., 2015). The importance of the instream atmospheric heat exchange is also supported by the high annual and diel temperature amplitudes (Table 1), in close correspondence to the observed air temperature amplitudes over the year (between 17.5 and 19.5 °C at the lower elevations, with a 30-day moving average).

4.3.2 Spring temperature

Regarding the temperature recordings in the sampled water sources (springs and groundwater), they show varying correlations with air temperature at the Auberge station (Table 1); PZ1 has the strongest correlations (R^2=0.80) and ICEC the weakest (R^2=0.56).

The GRAS spring is a permanent source of water but is small in volume, with an outflow of only a few liters per minute (personal observation). The temperature is recorded directly in the outflowing water, the sensor might thus heat up by atmospheric heat exchange in case of very low outflow rates. This most probably explains some strong sub-daily temperature fluctuations of the GRAS (and ROCK) springs (Figure 3). Despite these diel fluctuations, the GRAS temperature signal does not seem to react to the summer rainfall events (visible as peaks on the streamflow), whereas ROCK shows a reaction.

The shape of the temperature signal of the BRDG spring differs from the sinusoidal shape of the GRAS and ROCK springs (the shape of the air temperature variations). The BRDG spring signal shows a constant temperature during winter, with an increase during the early melt and melt periods, with e.g. a temperature rise from 4.3 °C to 5.4 °C over 3 weeks at the beginning of M2. The temperature rise stops around the time when soil temperature at mid-elevation shows snow disappearance (blue bar in Figure 3) and then recedes to winter base temperature. These two patterns (strong reaction during melt at low elevations,

https://doi.org/10.5194/hess-2022-48
Preprint. Discussion started: 8 February 2022


Hydrology and Earth System Sciences Discussions

return to a base temperature during winter) suggest that the BRDG spring is fed by snowmelt from low elevations (from the right bank riparian area where it is located) during spring and by groundwater the rest of the year.

All spring temperatures converge at around 4.3 °C at the end of B2 (the only winter period measured in all springs), which corresponds to the almost constant temperature of ICEC spring (annual amplitude of 0.4 °C, Table 1).

The two piezometers that access the groundwater (PZ1 and PZ3) are both located in the alluvial floodplain where the stream meanders. During intense rainfall events, PZ1 shows strong positive temperature excursions, which can even exceed streamflow temperature in summer; its winter anomalies are smaller. The annual cycle of the PZ1 temperature reaches its maximum temperature of 7.9 °C with a delay of 74 days (2.5 months) after the air maximum and exceeds the maximum recorded in the springs by 1.5 °C. The strong delay of the annual cycle together with the warm temperatures and relatively small amplitude dampening compared to ROCK and GRAS springs suggests that it is influenced by a large storage volume which induces the delay and is closely connected to heat input from the surface.

PZ3 shows the same annual temperature amplitude as PZ1 but has an even longer delay (21 days with respect to PZ1) and has a negative offset of 1.5 °C of its maxima (6.4 °C for PZ3) compared to PZ1, possibly related to the higher elevation and more northern aspect of its source area (PZ3 is located 30 m higher, in the more north-facing part of the catchment). PZ3 has, however an average temperature of 4.8 °C closer to the one of the springs.

A distinctive feature of PZ3 is its temperature decrease during M2, in phase (but in opposite direction) with the streamflow increase. This suggests a direct, relatively important cold input during snow melt, resulting from a high hydrologic connectivity of PZ3 to snowmelt water (either directly or via exfiltration from the stream) and a low storage volume during this time of the year.

Table 1. Statistics on temperature time series recorded in the stream, piezometers, and springs. The dampening depth estimated for the BRDG spring (*) is biased because of a positive anomaly of temperature due to snowmelt input (see text).

Water source	Mean T [°C]	Max T [°C]	Annual T amplitude [°C]	Max. diel T amplitude [°C]	Cross corr. w/ air T		Dampening depth [m]	Snowmelt anomaly	Rainfall anomaly
					Lag [days]	Max corr. [-]			
Stream	5.0		8.8	11.4	0	0.92	-	-	-
PZ1	6.3	7.8	3.8	4.0 (punctually)	79	0.80	3.2	No	Yes
PZ3	4.8	6.3	3.7	0.5 (punctually)	105	0.68	4.3	Negative	No
GRAS	5.5	7.4	3.0	2.4	41	0.76	1.7	No	Yes
ROCK	5.4	6.7	2.5	2.9	39	0.76	1.6	Positive	yes
BRDG	4.7	5.6	0.9	0.9	6	0.68	0.2*	Positive	No
ICEC	4.3	4.7	0.4	0.6 (noise)	133	0.54	5.4	No	No

4.3.3 Flowpath depth estimation

We can use a simple analytical temperature model with sinusoidal initial conditions (e.g. Elias et al., 2004) to compute a rough depth that would correspond to such a lag *L* (for details see Appendix 2). With a typical thermal diffusivity of soil of 5.56 10^{-}

https://doi.org/10.5194/hess-2022-48
Preprint. Discussion started: 8 February 2022


Hydrology and Earth System Sciences
Discussions

^{7} m^2/s (Elias et al., 2004) a lag of 41 days would correspond to a depth of 1.7 m, a lag of 39 days to 1.6 m. The dampening depths estimated for the other water sources are reported in Table 1. They should however be interpreted with care as i) the presence of an insulating snowpack on the hillslopes prevents heat advection during winter, thereby further increasing temperature lags and amplitude dampening in the subsurface, and ii) the model is only based on heat conduction and does not account for advection that could be locally important during snowmelt inputs.

Such limitation is reached at BRDG, as the temperature variation over the year (0.9 °C) happens over few weeks during melt periods (M1 and M2); this variation shows a strong reactivity to the snowmelt input but the resulting estimation of flowpath depth (0.2 m) is obviously erroneous. At this time, the maximum air temperature is not reached yet (during R2 and R3) and the expected heat signal transferred from air by conduction later in the year is finally not visible.

All subsurface water temperatures except one have a dampened annual cycle and a positive lag compared with streamflow temperature, which can be explained by the delay resulting from heat conduction (depending on the soil's thermal diffusivity *D*) and advection with water flow. The one exception is BRDG, for which lag estimation fails. The lags are furthermore coherent with the dampening: stronger lags correspond to stronger dampening and are associated with deeper depths.

4.4 Electrical conductivity

The electrical conductivity of all samples is high compared to what we could expect in an Alpine environment (Cano-Paoli et al., 2019). The median value of 216 µS/cm in the streamflow samples at the outlet (Figure 4 F) is not significantly different from the streamflow samples of the upper subcatchment (HyS2, median EC of 215 µS/cm); assuming a spatial homogeneity between flow path depth and flow velocity, this similarity suggests a similar flow path length distribution. The temporal evolution of EC in the stream shows a typical seasonal pattern (Penna et al., 2014; Cano-Paoli et al., 2019), with a decrease in EC during the melt season. A similar pattern was observed by Chiaudani et al. (2019) for a large aquifer in Italy, who explained that it results from the large amount of melt water that recharges into the aquifer and creates a decrease of electrical conductivity, resulting from a combined effect of volume increase and dilution. This dilution effect is obtained because any recharging water has a shorter subsurface residence time than old water and accordingly a lower ionic content and thus EC (Cano-Paoli et al., 2019). We furthermore observed a certain time lag between the seasonal cycles in EC and streamflow cycle (Figure 6), which was previously shown by Cano-Paoli et al. (2019). On an event-scale basis, a similar lag between streamflow and EC has been previously observed and is explained by the well-known delay between the transmission of pressure waves (leading to discharge increase) and the actual arrival of newly recharged water (Chiaudani et al., 2019). This event-scale lag will ultimately lead to a shift of the seasonal cycle of streamflow and EC.

All springs, except ICEC have higher EC values than the stream or the groundwater. Higher EC values point towards longer flow paths in the subsurface, either vertically or laterally (Cano-Paoli et al., 2019), or alternatively longer residence times of the water, hence lower flow rates. The spring with the highest EC (GRAS, median EC of 271 µS/cm) shows the least temperature dampening, and vice-versa, the spring with the lowest EC (ICEC, median 211 µS/cm) shows the most dampening (where high amounts of dampening indicates deep flow paths in the subsurface). Assuming an homogeneous underlying

https://doi.org/10.5194/hess-2022-48
Preprint. Discussion started: 8 February 2022

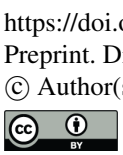

Hydrology and Earth System Sciences
Discussions
Open Access
EGU

geology, the only possible explanation of EC signals in conjunction with the temperature signals is thus that low EC values of subsurface water result from short flow paths in the shallow subsurface (GRAS spring), and relatively high EC values result from longer and deep flow paths (ICEC).

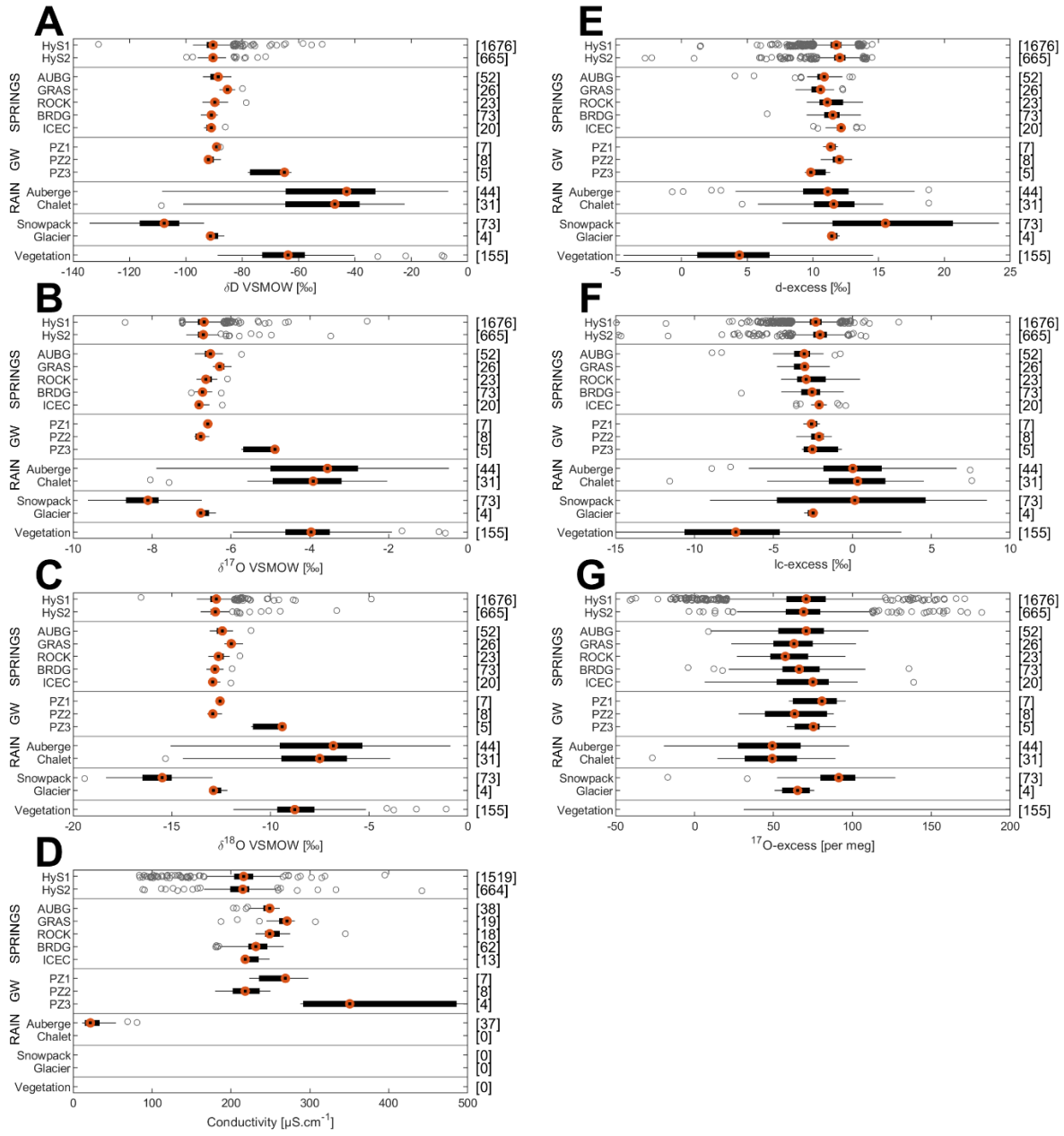

Figure 4. Range of δ^2H, $\delta^{17}O$, $\delta^{18}O$, conductivity, d-excess, lc-excess and ^{17}O-excess for stream, springs, groundwater, rainfall, snowpack, glacier and vegetation water samples. The left and right end of each box show the 25th and 75th percentiles, and the middle point is the median. The whiskers go up to 1.5 times the interquartile range; values beyond the whiskers (outliers) are marked with circles. The values on the right y-axis of the figures are the number of samples in each category. Note that there

https://doi.org/10.5194/hess-2022-48
Preprint. Discussion started: 8 February 2022


Hydrology and Earth System Sciences
Discussions

are no conductivity measurements for snowpack and vegetation water samples. For ^{17}O-excess the values of vegetations samples are out of the box (median 572 ‰, 25th and 75th percentiles are 374 ‰ and 742‰, resp., and whiskers are from 31 ‰ to 8329 ‰).

4.5 Stable isotopes of water

4.5.1 Ranges of δ^2H, δ^{17}O and δ^{18}O

The overall observed ranges of isotopic compositions (δ^2H, δ^{17}O and δ^{18}O values), d-excess, lc-excess, ^{17}O-excess and EC of all water samples are summarized in Figure 4 and their temporal evolution is shown in Figure 5, Figure 6 and Figure 7.

The sampled rain water has a lapse rate of 0.84 ‰/(100m) for δ^2H and 0.128 ‰/(100m) for δ^{18}O, which is approximately half the isotopic lapse rates of precipitation observed in Switzerland (e.g. Beria et al., 2018), with an ensuing higher median value at the lower Auberge weather station.

This lapse rate does not show up in the stream water (Figure 4 a, b, c). A rough computation (see also Appendix 3) shows that the distribution of elevations connected to HyS1 is not sufficiently different from the distribution at HyS2 to lead to a significant off-set of the isotopic values at the two streamflow sampling locations, despite the isotopic lapse rate. This most likely also explains the similar median isotopic values of all sampled water bodies, except the GRAS spring, with a significantly higher median value. This suggests that this spring might receive water only from a small low elevation subcatchment and not from the high rock walls located next to it.

The median δ^{18}O value of all streamflow samples equals -12.7 ‰, which is in line with the slightly lower values observed for the Rhone in Porte de Scex (Schurch et al., 2003), of which Vallon de Nant is a headwater catchment (albeit one with relatively low elevations compared to other headwater catchments of the Rhone).

https://doi.org/10.5194/hess-2022-48
Preprint. Discussion started: 8 February 2022

Hydrology and Earth System Sciences
Discussions
Open Access
EGU

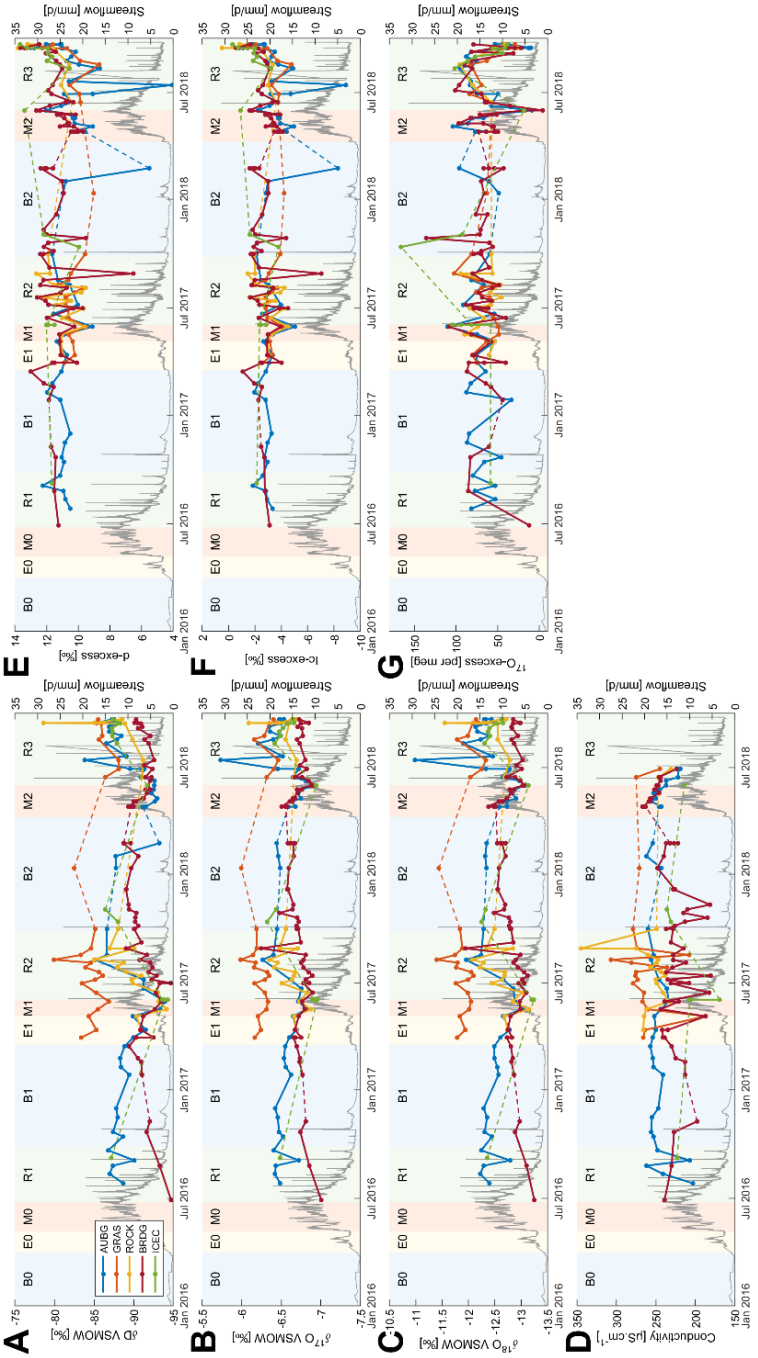

Figure 5. Time series of δ^2H, $\delta^{17}O$, $\delta^{18}O$, conductivity, d-excess, lc-excess and ^{17}O-excess for 5 springs (location on map Figure 1 A).

https://doi.org/10.5194/hess-2022-48
Preprint. Discussion started: 8 February 2022

Hydrology and Earth System Sciences
Discussions
Open Access
EGU

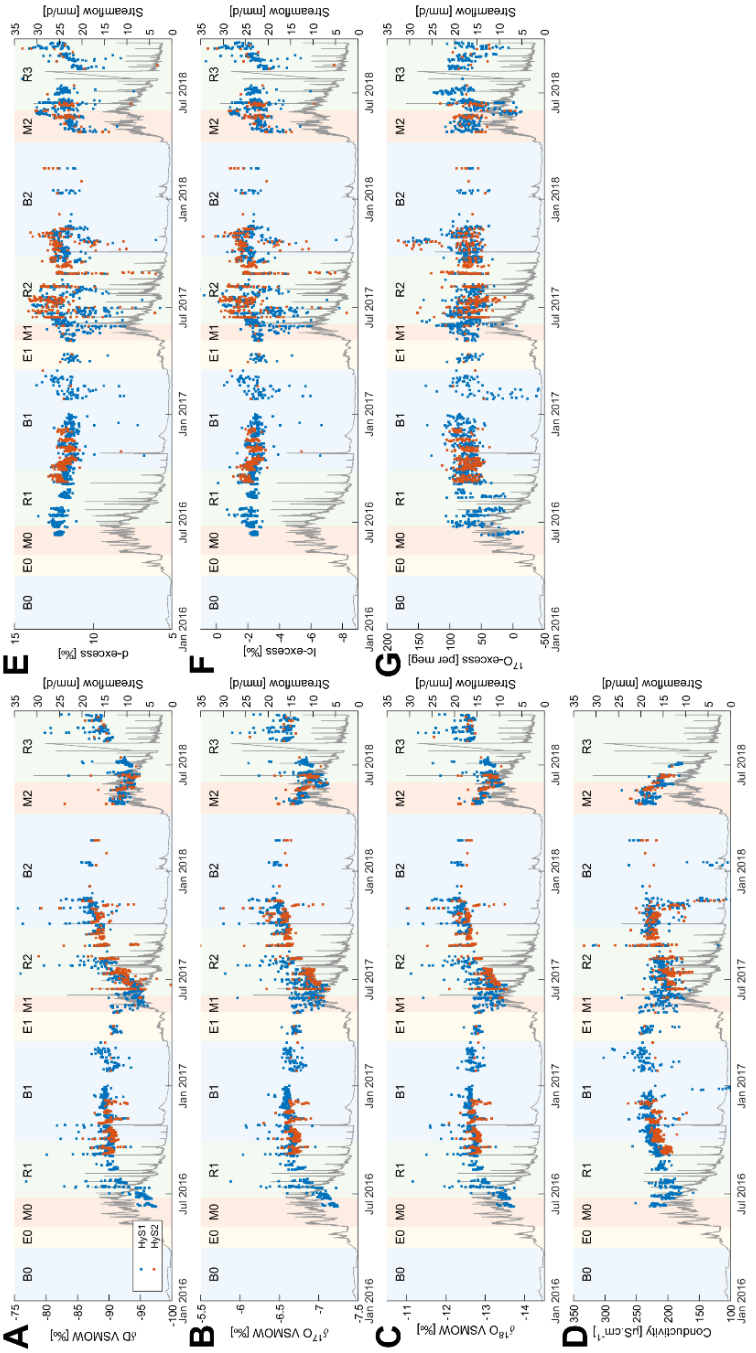

Figure 6. Time series of δ^2H, $\delta^{17}O$, $\delta^{18}O$, conductivity, d-excess, lc-excess and ^{17}O-excess at the Vallon de Nant outlet HyS1 and at the upper subcatchment HyS2 (location on map Figure 1 A).

https://doi.org/10.5194/hess-2022-48
Preprint. Discussion started: 8 February 2022

Hydrology and Earth System Sciences
Discussions
Open Access
EGU

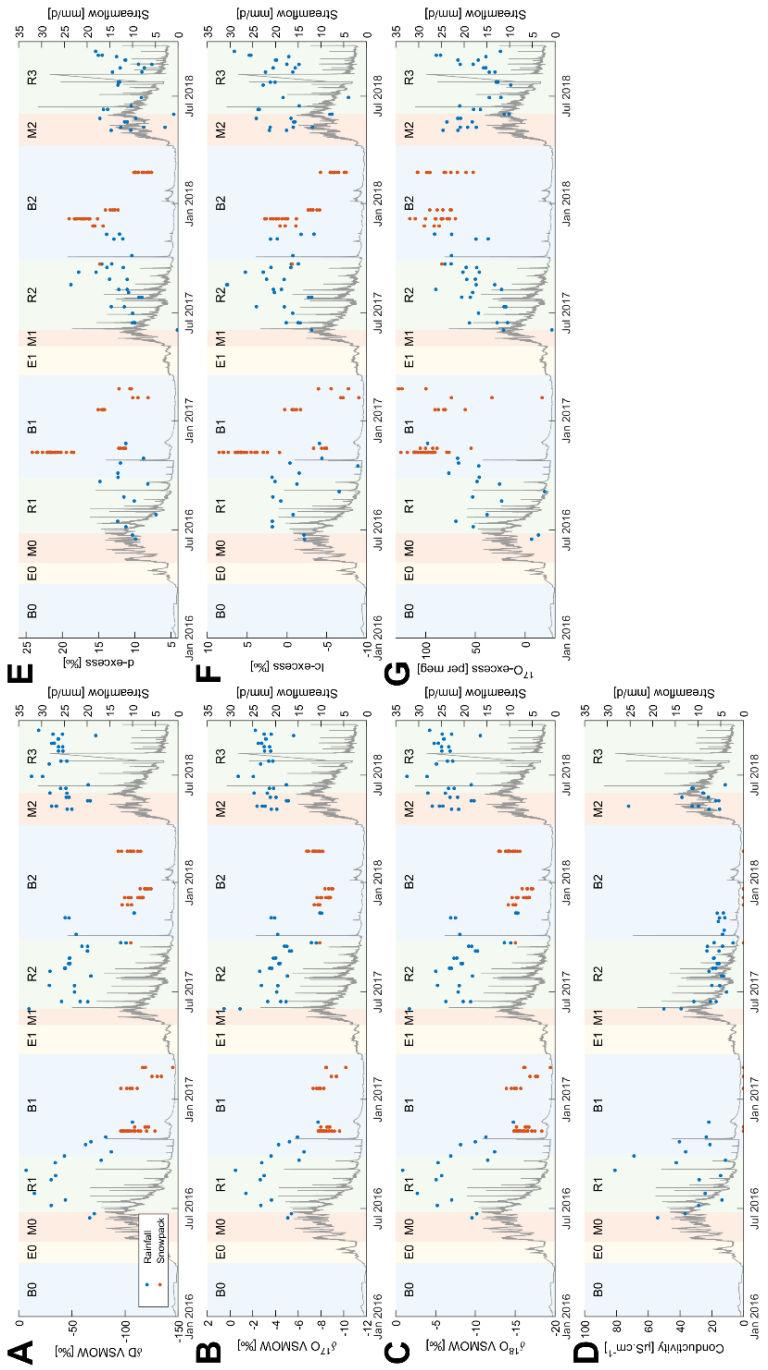

Figure 7. Time series of δ^2H, $\delta^{17}O$, $\delta^{18}O$, conductivity, d-excess, lc-excess and ^{17}O-excess for rainfall (from Auberge and Chalet weather stations, location on map Figure 1 A) and snowpack. Note that the conductivity of snowpack has not been measured.

https://doi.org/10.5194/hess-2022-48
Preprint. Discussion started: 8 February 2022


Hydrology and Earth System Sciences
Discussions

425 **4.5.2 Dynamics of δ^2H, $\delta^{17}O$ and $\delta^{18}O$ in springs**

The fluctuations of the isotopic composition from 6 springs monitored between July 2016 and September 2018 is discussed qualitatively based on the streamflow periods (see Figure 5). The relative variations being similar between δ^2H, $\delta^{17}O$ and $\delta^{18}O$, only the $\delta^{18}O$ variations are commented hereafter.

Despite some variability, the AUBG spring $\delta^{18}O$ values remain relatively constant ($\delta^{18}O$ between -12.8 ‰ and -12.2 ‰) during
430 the 2016 streamflow recession R1 and then slowly decrease throughout the 2016/2017 baseflow period B1. Meanwhile, the BRDG spring starts with more depleted isotopic values (-13.3 ‰) but get enriched in the heavy isotopes through R1 and B1 to finally have a similar composition during the 2017 early melt period (E1) compared to the AUBG (and ROCK) springs, also with a subsequent decreasing trend in the heavy isotopes.

The 2017 minimum isotopic values of the AUBG, ROCK and BRDG springs are reached around the time of 2017 maximum
435 streamflow and then diverge during the 2017 recession period (R2), increasing at a different rate: the δ-values of AUBG and ROCK springs increase quickly (+1.0 ‰ in 3 months), while the BRDG spring values only initiates a slow increase that will continue throughout winter (B2).

The beginning of the 2018 melt period was exceptionally fast, without an early melt period. The springs sampling started 3 weeks after it's the beginning of the early melt period, with a significant part of the snowpack having melted already. As during
440 M1, the isotopic composition of the AUBG and BRDG springs over this period shows a constant decrease in the heavy isotopes until the 2018 streamflow maximum. At the inverse of R1, the BRDG composition then remains constant during the recession, while the AUBG spring increases quickly in the δ-values.

The pattern repeats during the 2018 melt period (M2) with a decrease in δ-values, which then diverge at different rates. Again, the BRDG spring δ-values increases slowly, while for the AUBG and ROCK springs the increase is faster.

445 The ICEC spring, located on the western slopes (Figure 1), tends to follow the same isotopic pattern as the AUBG spring. Although, because of its lower sampling rate, points are missing at the critical moments during the melting periods, and so we cannot discuss the differences in timing. It can be pointed out also that ICEC shows higher isotopic values compared to BRDG even if it is located at a higher elevation. This can be explained by the higher maximum elevation of the mountain ridge upstream of BRDG compared to ICEC (see Figure 1), which most certainly leads to a higher snowfall proportion for BRDG.

450 As discussed earlier, the GRAS spring behaves differently from other springs, with higher δ-values than all the others in 2017. EC and temperature measurements indicate that this spring has relatively shallow flow paths and its δ-values also suggest a larger proportion of rainfall-derived water (which has a higher average δ-values than snowmelt)

4.5.3 Dynamics of δ^2H, $\delta^{17}O$ and $\delta^{18}O$ in streamflow

The temporal evolution of the isotopic ratios in the streamflow shows high δ^2H values during winter baseflow, close to the
455 median value of all sampled subsurface water bodies, and a significant decrease in the heavy isotopes during the melt periods.

https://doi.org/10.5194/hess-2022-48
Preprint. Discussion started: 8 February 2022


Hydrology and Earth System Sciences
Discussions

Streamflow is thus largely fed by recent (isotopically light) snowmelt during the melt period; the decrease of the δ-values is proportional to the amount of snowmelt, with a larger decrease in 2017 compared to 2018.

The early melt period does not decrease the δ-values, which suggests that during this period, the streamflow is composed of previously stored groundwater and not of recent, mid-winter snowmelt at hydrologically close areas (e.g. in the floodplain or the riparian area), as is assumed in some models (Schaefli et al., 2014).

4.5.4 d-excess

The sampled rainfall has a median d-excess of 11.3 ‰, which is in the range of published values for rainfall in the Swiss Alps (Leuenberger and Ranjan, 2021). The snowpack samples have a median value of 15.5 ‰. Values from the Swiss Alps (Grimsel, Schotterer et al. (2004)) show similarly high d-excess values in winter. High d-excess from snowpack is caused by the assumed source of winter precipitation, the Mediterranean Sea (Froehlich et al., 2002). Secondary evaporative process happening within the snowpack or on the snowpack surface led to a further shifting away of the isotopic ratios from the GMWL, i.e. to a decrease of the d-excess values. Since we did not sample fresh snowfall but from the snowpack, we can safely assume that the original fresh snow in our catchment could have even higher d-excess values. Secondary evaporation effects also explain the low d-excess values for the glacier ice samples.

The surface and subsurface water samples show d-excess median values close to that of rainfall and considerably lower than the median value for snow. The apparent surface and subsurface water samples bias towards the d-excess value of rain can be explained by secondary evaporation (from the soil or vegetation); the soil water that remains (and that ultimately recharges groundwater and the streams) thus has a lower d-excess value than either rainfall or meltwater. This process also explains the low d-excess values of xylem water in vegetation.

The above illustrates that d-excess values are rather difficult to interpret in terms of local scale process information ; the significant difference between the values for rainfall and snow pack indicates some potential to quantify snowfall and rainfall proportions in streamflow but secondary evaporative processes prevent a straight forward estimate. For ice melt, d-excess values are too close to those of rainfall for providing further insights into its importance in streamflow.

4.5.5 LC-excess

Figure 4 F shows the computed LC-excess values. The range of values for the rainfall samples are related to the spread around the evaporation line. We see that the median value of the snowpack samples is close to the reference for rainfall (0 ‰), which is in line with the findings Beria et al. (2020) who reviewed snowpack data for entire snow seasons and does often not show a significant deviation from median values for the reference precipitation value. On average, secondary snow evaporation does not appear to be important in our catchment. The xylem water samples from larch trees show the expected low LC-excess values due to strong evaporation effects.

All subsurface water and stream samples have a negative median value, indicating that all recharged water in this catchment has undergone evaporation, albeit at degrees that vary in space and time. Compared to other subsurface samples, the ICEC

https://doi.org/10.5194/hess-2022-48
Preprint. Discussion started: 8 February 2022


Hydrology and Earth System Sciences
Discussions

spring samples seem to be less affected by evaporation (has a higher LC-excess value), which agrees with the fact that the area upstream of this spring is occupied by only low growing vegetation (meadow and shrubs) and that for this spring the rainfall is directly exfiltrated.

4.5.6 ^{17}O-excess

Our computed ^{17}O-excess values of rainfall (Figure 4 G) are much higher than the few published values in Switzerland, which range from 6.5 per meg (Leuenberger and Ranjan, 2021) to 18 per meg (Affolter et al., 2015) for low and high elevation locations. There are no published values for snowfall or snowpack for Switzerland, but values between 17 and 62 per meg for freshly precipitated snow on Mount Zugspitze (German Alps, 2,962 masl) are found in the work of Surma et al. (2021). Our values for snow have a median value of 91.3 per meg and are significantly higher than for rainfall (49.2 per meg).

The difference between rainfall, snowpack and glacier observed for δ^2H, δ^{17}O and δ^{18}O is also visible with ^{17}O-excess, but not with d-excess. ^{17}O-excess could potentially be useful to distinguish between rainfall, snowpack and icemelt but secondary evaporative processes complicate a direct interpretation.

Given that the local and global reference lines for ^{17}O are very similar (see Section 3.1), it is tempting to interpret the spatial differences in ^{17}O-excess values; the median values of all sampled water show a coherent picture, with subsurface and stream water having intermediate values between rainfall and snow samples and thus being a mix thereof. As for d-excess, we can however not draw any direct conclusions on mixing ratios since rainfall and snowfall undergo further evaporative processes during recharge.

Furthermore, the temporal dynamic of ^{17}O-excess in springs does not show additional information compared to d-excess. Given the lack of reference data at comparable sites, we cannot elaborate further at this stage.

5 Discussion

Below we discuss how the above findings contribute to answer our research questions on the origin of streamflow and on the role of subsurface flow.

5.1 Origin of winter streamflow

The streamflow in the studied catchment shows the typical seasonal recession leading to an almost constant winter baseflow between January and March. It is tempting to assume that such catchments are essentially dormant during winter (Schaefli et al., 2013) without any liquid water input, and thus to use the constant end of winter baseflow to infer total storage (Cochand et al., 2019). However, we observed diverging isotopic ratios in two springs, showing either an enrichment in heavy isotopes (AUBG) or an enrichment in light isotopes (BRDG) during winter (Figure 5). Such an enrichment by light isotopes can only be explained by the presence of winter melt processes feeding light isotopes throughout the winter to the respective groundwater system.

https://doi.org/10.5194/hess-2022-48
Preprint. Discussion started: 8 February 2022


Hydrology and Earth System Sciences Discussions

The result is also supported by the relatively constant EC value of the AUBG spring: in absence of any inflow, we would expect a gradual aging of the water and thus an increase of EC. Therefore, assuming the water is not saturated with regards to the ionic charge, a constant value suggests a permanent new water input (with low EC) during winter. Thus, in the Vallon de Nant, winter base flow is the combined result of the long seasonal recession and some small input during winter; whether this input is related to air-induced snowmelt or ground heat melt (Schaefli, 2016) remains to be investigated.

5.2 Dominant runoff processes driving streamflow generation during early spring snow melt

The start of the two early melt streamflow periods corresponds to the disappearance of snow at the lowest soil temperature measurement point (1,240 masl). This suggests that this early melt streamflow rise might well be linked to local snowmelt water input to the stream at the lowest elevation. At the same period, at higher elevations, the snow cover is still in place (according to the soil temperature observations). It is unknown whether snow melt is already occurring at these higher elevations during the early melt period since potential snow melt might most probably be retained in the existing snowpack or in the subsurface.

Furthermore the streamflow increases at the beginning of E1, but that the decrease of EC is delayed (Figure 5), suggesting that older water (with high EC) is pushed into the stream at the beginning of E1. This is consistent with the unchanged isotopic composition of streamflow during E1, showing that streamflow input is dominated by groundwater during this period.

5.3 Dominant runoff processes during melt periods

Although the δ^2H, $\delta^{17}O$ and $\delta^{18}O$ annual medians of AUBG, ROCK, BRDG and ICEC show an enrichment in the light isotopes with elevation (Figure 4), these values are difficult to compare due to the number of samples and the sampling dates that vary by source. However, we notice in Figure 5 that the isotopic compositions of these 4 water sources converge towards a common value during M1 (around -93.5 ‰ for δ^2H, -6.8 ‰ for $\delta^{17}O$ and -13.0 ‰ for $\delta^{18}O$), which suggests that the entire subsurface is flushed with snowmelt that either comes from a similar elevation range or that sampled all elevation ranges in a similar way. The higher EC values in the stream compared to the springs during the melt period (Figure 5, Figure 6) are unexpected: it suggests that there is a significant amount of subsurface water reaching the stream that has a higher EC value than all sampled springs. This result however underlines the importance of subsurface flow paths during melt periods.

The positive temperature anomalies (during summer rainfall events) observed during M2 (ROCK) shows the existence of fast surface flowpaths but are not enough to explain the high EC values at this period.

5.4 Dominant runoff processes during the seasonal recession

The divergence of the isotopic composition of the four springs (AUBG, ROCK, GRAS and BRDG) after the melt period (due to increased summer rainfall contributions) give clues, qualitatively, either about their respective reservoir size or about their respective relative permeabilities and/or outflow rates: a smaller increase in δ-values indicates hereby a larger reservoir or

https://doi.org/10.5194/hess-2022-48
Preprint. Discussion started: 8 February 2022


Hydrology and Earth System Sciences
Discussions

slower flow rates/permeabilities (e.g. BRDG); a relatively rapid increase in values is associated to a small reservoir size or to high permeabilities/flow rates (e.g., AUBG).

The EC increase of springs and streamflow during R2 shows the prevalence of deeper flowpaths, as the stream water get less diluted by the shallow and faster flowpaths (low EC) from snowmelt contribution.

5.5 Interplay of shallow groundwater in the hillslopes and of alluvial or talus groundwater systems

During M2, both BRDG and PZ3 temperature signals are correlated with streamflow variations, but the positive temperature anomaly measured at BRDG suggests a snowmelt input that is heated up before infiltration (due to heat exchange during surface runoff), while the negative temperature anomaly for PZ3 suggests the melted snow is directly infiltrating. Indeed, the subcatchment area of BRDG collects snowmelt from the nearby riparian area and steep slopes facing west that are exposed to sun radiation, while the temperature anomaly for PZ3 begins with the melt period start and ends approximately when the area is free of snow (200 m from soil temperature sensor at 1,530 masl), which suggest a local infiltration of snowmelt. The water temperature is usually influenced by ground temperature, but the high hydraulic conductivity in the area of PZ3 probably does not allow time for the water temperature to reach equilibrium. This temporary (6 weeks) and local snowmelt input is superimposed on a longer scale pattern that leads to 74 days of lag between PZ3 and air temperature. This suggest that we have here a groundwater system that is very well connected to surface water during the melt period, but with a much more dampened response later in the year.

The PZ1 (470 m to the north) reacts in a different way: the 58 days of lag indicate a shallower flow path, but without temperature anomaly during the melt period. Short-term temperature anomalies (positive during the summer, negative during the winter) associated with rainfall events suggest local incursions of surface water, which is however in contradiction with the absence of temperature anomalies during the melting period. One possible explanation is that the stored water volume is small enough (with water levels between 0.8 and 2.4 m below the surface, see Supplementary Material, Figure S8) during R2 and B2 to react quickly to local surface inputs, while during M2 the stored volume is high enough (with water level between 0.1 and 1.0 m below the surface) to not show short term reactions to melt water input.

The average temperature difference between PZ1 and PZ3 (mean 6.3°C and 4.8 °C over the year) can most likely be explained by their respective subcatchments: PZ1 (left bank) collects water from the grassy slopes of the west side of the valley (facing east), while through PZ3 (right bank) flows water from the south (facing north), with more shaded areas and snowpack remaining later in the year.

At the end of B2, the 4 springs tend to converge to a temperature around 4.3°C and if we limit ourselves only to this variable, we could think that this is pointing toward a common aquifer feeding them during baseflow. The shift of the PZ1 and PZ3 temperatures (+0.4 °C and -0.5 °C) at the end of baseflow could be explained by a calibration issue. The fact that streamflow isotopes during B2 are close to the median value of all sampled water sources suggests that our spatial sampling was good enough to represent the main water sources during baseflow.

https://doi.org/10.5194/hess-2022-48
Preprint. Discussion started: 8 February 2022


Hydrology and Earth System Sciences
Discussions

The available EC measurements clearly suggest that the subsurface flowpath distributions are very similar in the upper part of the catchment (HyS2) and in the lower part of the catchment (HyS1). This is supported by the fact that the isotopic lapse rate observed in rain water does not show up in streamflow.

The isotopic composition of GRAS is quite different from that of the other sources (mean values of -85.3 ‰ for δ^2H, -6.3 ‰ for $\delta^{17}O$ and -12.0 ‰ for $\delta^{18}O$). The absence of a temperature anomaly during the melt period suggests a large and well-mixed source of water. The high thermal connectivity with the surface could then be explained by a shallow flowpath over a certain distance before the water exits at the source. However, we still cannot explain why the temperature signal shows a variation induced by rainfall, whereas there is no variation due to snowmelt input.

5.6 Transferable insights into the value of the observed variables for hydrologic process investigations in comparable catchments.

5.6.1 Water sources temperature and shallow soil temperature

Although temperature is not a conservative tracer, temperature measurements of springs are very useful to estimate flowpath depth. However, the underlying assumption that heat transfer is essentially driven by conduction might not always be verified (Kane et al., 2001), and anomalies between measured and modelled temperature (pure sinusoid) could be related to heat transport with subsurface water flows (i.e. to advection phenomena).

At shallow depth (10 cm), the soil temperature is strongly influenced by air temperature, and the present analysis of soil temperature at different elevations shows that it is a good proxy for the detection of snow cover. Early melt starts when the soil temperature at low elevation (1,240 masl) rises, showing that snow is melting in the area close to the outlet (1,200 masl). The temperature sensor, albeit not intended for this use, seems to be well positioned to detect the onset of early melt for the melting seasons in 2016 and 2017 (no early melt in 2018).

For the other soil temperature recordings, there is no direct link to the streamflow dynamics. The time elapsed between the snowmelt onset on the next higher soil temperature site (1,530 masl) and the beginning of the melting period varies significantly but is always positive (8 days in 2016, 3 days in 2017 and 51 days in 2018). The large variations of this lag time tend to indicate that the snowpack disappearance might not be a good proxy for actual snowpack melt outflow. Indeed, the underlying assumption is that snowpack disappearance might follow a similar pattern from one year to the other, but it does not consider the area which is actively melting and supplying melted snow, nor snowpack thickness.

A larger number of soil temperature sensors would provide an interesting perspective to identify more precisely the relative contributions of the different landscape units, elevations, and terrain aspects. This could be particularly promising in combination with satellite images for snow cover mapping.

5.6.2 Isotopic composition of springs and stream water

Stable isotopes of water are particularly promising to track the co-existence of seasonal baseflow and winter melt within springs and shallow groundwater. However, this requires year-round time series to understand which locations become

https://doi.org/10.5194/hess-2022-48
Preprint. Discussion started: 8 February 2022


Hydrology and Earth System Sciences
Discussions

enriched in heavy isotopes with time throughout the winter and which ones become depleted. This year-round monitoring is particularly important since, as we have shown, many subsurface signals are likely to see a "reset" during the main melt period. The range of isotopic composition for each source informs on the relative snowmelt proportions from their respective subcatchments. Without evidence of a strong isotopic lapse rate in snowfall, the differences measured can be explained by the variation of snowfall amounts with elevation.

The relative proximity of some water sources monitored in this study underlines that spatial proximity does not necessary imply similar behaviours (in terms of temperature or isotopic composition), as we see noticeable differences between the sources due to the different characteristics of their subcatchments (i.e. flowpath depth, hydraulic conductivity, slope ,aspect). LC-excess values might reveal some additional insights in future work, in combination with future analyses of soil water isotopes (to give insights into evaporation effects).

At this stage, it is not clear either what the value of ^{17}O-excess is for hydrological purposes and the question whether it conveys local scale information remains open. These measures would have probably been more relevant if fresh snow was sampled instead of the snowpack. Even if we cannot draw any interesting conclusions, the publication of these values will nevertheless be useful for future work.

5.6.3 The added value of EC

EC allows a qualitative estimation of the water age, but the difficulty to characterize the different physical and geochemical properties of soils (influencing EC) do not allow an intercomparison of absolute EC values between the sources. However, the variations at a given source may inform on the snowmelt input (low EC) or the flowpath dynamic (old water pushed by water input). Especially in catchments that, similarly to ours, show little elevational gradients in the isotopic ratios of different water sources, EC represents an extremely valuable tracer to observe in addition to isotopes and water temperature, i.e. when having changes in EC which are not following the changes in the isotopic composition.

6 Conclusion

We presented a detailed study on the interplay of hydrological processes across all streamflow seasons of a high Alpine catchment, with the help of temperature recordings and measurements of EC and of stable isotopes of water. The combined use of these three natural tracers has been shown to be very promising to analyze the temporal succession of surface and subsurface runoff contributions to streamflow, specifically around the "reset" of the isotopic composition during the melt period. The range of the isotopic composition of each source also informs on the relative proportions of snowmelt.

Our study of the isotopic composition of streamflow as well as of EC values suggest that i) subsurface flow plays a prominent role throughout all stages of the melt period and that ii) winter streamflow might be partially fed by winter snowmelt and not by groundwater alone. Subsurface flow and winter melt might thus require more specific attention during future hydrologic model development.

https://doi.org/10.5194/hess-2022-48
Preprint. Discussion started: 8 February 2022


Hydrology and Earth System Sciences
Discussions

Water temperature recordings have been shown to be particularly useful to trace the subsurface water, specifically the relative depth of different subsurface water sources and how well the reservoirs are connected to the atmospheric heat input; it has a particular added value when it is measured jointly with EC because it disentangles shallow flow paths from deeper flow paths (which both can lead to a high EC signal). These results show the interest of monitoring the temperature of each potential water source, as this measure is simple and gives solid insights about the water flowpaths. In particular, temperature recordings in springs together with elevation distributed soil temperature monitoring is extremely powerful. However, future monitoring strategies should pay more attention to EC monitoring to obtain estimates of the water age.

Much laboratory time was devoted here to the measurement of $\delta^{17}O$ and ^{17}O-excess, without providing conclusive insights in their added value for local-scale snow hydrological processes studies, except some potential to distinguish glacier melt from snowmelt. This is partly also due to absence of relevant reference data. We hope that the full value of the $\delta^{17}O$ data set presented here will be unravelled in the future.

https://doi.org/10.5194/hess-2022-48
Preprint. Discussion started: 8 February 2022


Hydrology and Earth System Sciences
Discussions

Data availability. Stable water isotopes and conductivity measures of each water sample used for this paper is available online at https://doi.org/10.5281/zenodo.5940044.

Author contributions. AM and NC conceived the field study; AM, NC, HB and JL collected and analyzed the field data; AM, NC and HB did all the lab work; all authors discussed and interpreted the data; AM produced all computations and figures and, together with BS and TV led the writing of the paper.

Competing interests. Author Bettina Schaefli is a member of the editorial board of the HESS journal, but otherwise, there are no other competing interests of which the authors are aware.

Financial support. This research has been supported by the Swiss National Science Foundation (SNSF; grant no. PP00P2_157611).

Acknowledgement. Thank you to Lionel Benoît, Tristan Brauchli, François Mettra, James Thornton, Inigo Irarrazaval Bustos, Tom Müller, Pascal Egli, Loïc Perez, Aurélien Ballu, Judith Eeckman, Mirjam Scheller, Marvin Lorff, Rokhaya Ba, Anham Salyani, Guillaume Mayoraz, Raphaël Nussbaumer, Emily Voytek, Micaela Faria, Michael Rowley, Guillaume Gavillet, Gelare Moradi, Gabriel Cotte and Moctar Dambele for their precious help on the field. Thank you for Markus Randall and Loïc Perez for their help measuring electric conductivity in the lab.

https://doi.org/10.5194/hess-2022-48
Preprint. Discussion started: 8 February 2022

Hydrology and Earth System Sciences
Discussions

Appendix 1: Influence of air on the isotopic composition of a water sample (δ^2H, $\delta^{17}O$ and $\delta^{18}O$) within a sealed container

The purpose of this calculation is to estimate how the isotopic composition of a water sample locked up together with some air in a sealed container will be altered by the water vapor of the air. This configuration may happen i.e. with snow sampling as snow density ranging from 0.55 to 0.83 suggests that at least 17 % to 45 % of the volume in the container is ambient air from the sampling site. To make these calculations we consider the conditions in which the samples will be analysed; we take the ambient temperature of 25.3 °C for which we know the isotopic fraction factor between vapor and liquid phases of water for δ^2H, $\delta^{17}O$ and $\delta^{18}O$. At this temperature the samples are in a liquid phase, and in equilibrium with the air of their container. Following Mook et al. (2008), the isotopic fractionation of water between two phases at the equilibrium is written as a reaction between the liquid l and vapor v phases of H_2O as:

$$H_2O_l + H_2O^*_v \leftrightarrow H_2O^*_l + H_2O_g, \quad (1)$$

where * marks the heavy isotopic form of the molecule that may contain ^2H, ^{17}O or ^{18}O, and δ^* its isotopic composition in per mil. At a given temperature *T*, the isotopic fractionation factor of water between liquid and vapor $\propto_{l/v}$ is the equilibrium constant of the Equation 1:

$$\propto_{l/v}(T) = \frac{[H_2O^*]_l[H_2O]_v}{[H_2O]_l[H_2O^*]_v} = \frac{\delta^*_l/1000+1}{\delta^*_v/1000+1} \quad (2)$$

As we know i) the amount of liquid water in the container and its initial isotopic composition, ii) the amount of ambient air captured in the container and its initial isotopic composition, and that we can deduce iii) the total amount of heavy isotopes in the total amount of water, we can solve the Equation 2 as a second order equation.

The calculations are made for two extreme amounts of air vapor saturation, namely air without any water vapor and air fully saturated with water vapor. For the last one we take the partial pressure of water at 25°C P=3169.9 Pa (Haynes et al., 2017):

The value of the fractionation factor of water ^2H and ^{18}O between 0 and 100°C are (Majoube, 1971):

$$ln\ {}^2\propto_{l/v}(T) = 24.844.10^3/T^2 - 76.248/T - 52.612.10^{-3} \quad (3)$$

$$ln\ {}^{18}\propto_{l/v}(T) = 1.137.10^3/T^2 - 0.4156/T - 2.0667.10^{-3} \quad (4)$$

From Equations 3 and 4 we compute ${}^2\propto_{l/v}(T = 25.3\ °C) = 1.0789$ and ${}^{18}\propto_{l/v}(T = 25.3\ °C) = 1.0135$.

For ^{17}O we will take the experimental values given by Barkan and Luz (2005) at 25.3 °C: ${}^{17}\propto_{l/v} = 1.00496 \pm 0.00002$.

For each stable water isotope, the values are calculated for 2 extreme sample isotopic composition from our database (δ^2H = -180 ‰ and 5 ‰, $\delta^{17}O$ = -12 ‰ and 0 ‰, $\delta^{18}O$ = -30 ‰ and 5 ‰). The range of the isotopic composition of ambient air is based on records reported by Wei et al. (2019) for Rietholzbach, Switzerland (755 masl) from August to December 2011: the δ^2H air values range between -239.79 ‰ and -73.48 ‰, and $\delta^{18}O$ values range between -31.41 ‰ and -9.94 ‰. No reference value is available for $\delta^{17}O$, so a range between -30 and 0 ‰ has been chosen arbitrarily.

https://doi.org/10.5194/hess-2022-48
Preprint. Discussion started: 8 February 2022

Hydrology and Earth System Sciences
Discussions

The Figure 8 shows the changes of the sample isotopic composition for δ^2H, $\delta^{17}O$ and $\delta^{18}O$. These values have been completed for different amounts of air (ratios of sample volume over container volume).

The constant error for dry air corresponds to the case where the water vapor in air originates via evaporation of the water sample.

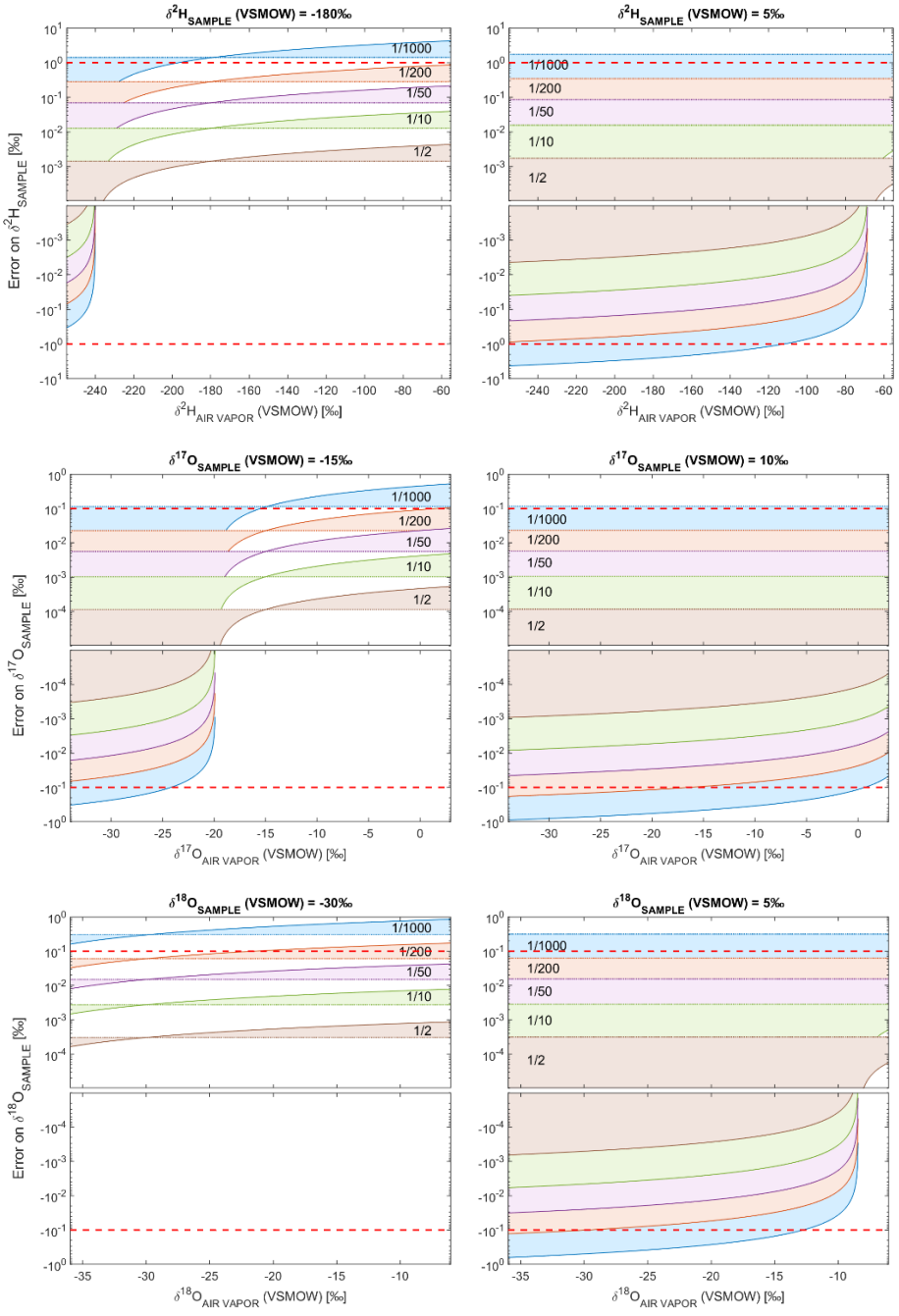

https://doi.org/10.5194/hess-2022-48
Preprint. Discussion started: 8 February 2022

Hydrology and Earth System Sciences
Discussions
Open Access
EGU

Figure 8. Changes in $\delta^{2}H$, $\delta^{17}O$ and $\delta^{18}O$ of a water sample depending on the initial isotopic composition of the water vapor of the air locked up with the sample. The results are completed for saturated air (continuous line) and dry air (dashed line), for
745 ratios of sample volume over container volume from 1/2 to 1/1000. The red dashed line represents the detection limit of the measuring device.

https://doi.org/10.5194/hess-2022-48
Preprint. Discussion started: 8 February 2022

Hydrology and Earth System Sciences
Discussions

Appendix 2: Estimate of water flow depth based on a soil temperature model

The estimate of the water flow depth is based on the soil temperature model presented in the work of Elias et al. (2004), assuming the water temperature measured at the spring/piezometer being equal to the soil temperature at the mean water flow depth. The evolution with time *t* of soil temperature *T* at the surface (depth *z=0*) corresponds to air temperature, and is characterized by the mean air temperature T_a and its amplitude *A*:

$$T(z=0, t) = T_a + A \sin(\omega t + \varphi), \quad (4)$$

with ω the radial frequency (in rad/s) and φ a phase constant (in rad). The heat transfer into the soil is dampened by *D*, the dampening depth coefficient (in m) expressed as a function of K (in m^2/s) the soil thermal diffusivity:

$$D = \sqrt{\frac{2K}{\omega}}, \quad (5)$$

giving the soil temperature at depth z:

$$T(z, t) = T_a + A \exp\left(-\frac{z}{D}\right) \sin\left(\omega t - \left(\frac{z}{D}\right) + \varphi\right), \quad (6)$$

The lag time *L* between air temperature and soil temperature at a given depth z is then:

$$L(z) = \frac{z}{\omega D}. \quad (7)$$

The depth is approached using the *fminsearch* function in MatLab, reducing the error between the observed lag time and the modelized lag time. Although the thermal diffusivity of soil is influenced by i) water volumetric content, ii) volume fraction of solids, and iii) air-filled porosity (Ochsner et al., 2001), we retain for this computation a unique value of thermal diffusivity of soil for all the points, using the typical value of $5.56.10^{-7}$ m^2/s (Elias et al., 2004). The sinusoidal air temperature is based on time series from a grided product (1 x 1 km grid) from MeteoSuisse (Schaefli, 2021). The results are presented in Table 2 and Figure 9.

Table 2. Characteristics of the sinusoidal air and water temperatures used for the soil temperature model, and characteristics of the soil temperature at the estimate depth corresponding to the water temperature.

Water sources	Measured air T [°C]		Measured water T [°C]		Air/Water lag time [d]	Modelized soil T [°C]		Modelized Soil depth [m]
	mean	*amplitude*	*mean*	*amplitude*		*mean*	*amplitude*	
PZ1	5.8	10	6.3	3.8	79	6	5.1	3.2
PZ3	5.8	10	4.8	3.7	105	4.5	3.3	4.3
GRAS	6.3	10	5.5	3	41	5.3	9.9	1.7
ROCK	6.3	10	5.4	2.5	39	5.2	10.2	1.6
BRDG	5.8	10	4.7	0.9	6	5	18	0.2
ICEC	5.8	10	4.3	0.4	133	4.2	2	5.4

https://doi.org/10.5194/hess-2022-48
Preprint. Discussion started: 8 February 2022

Hydrology and Earth System Sciences
Discussions

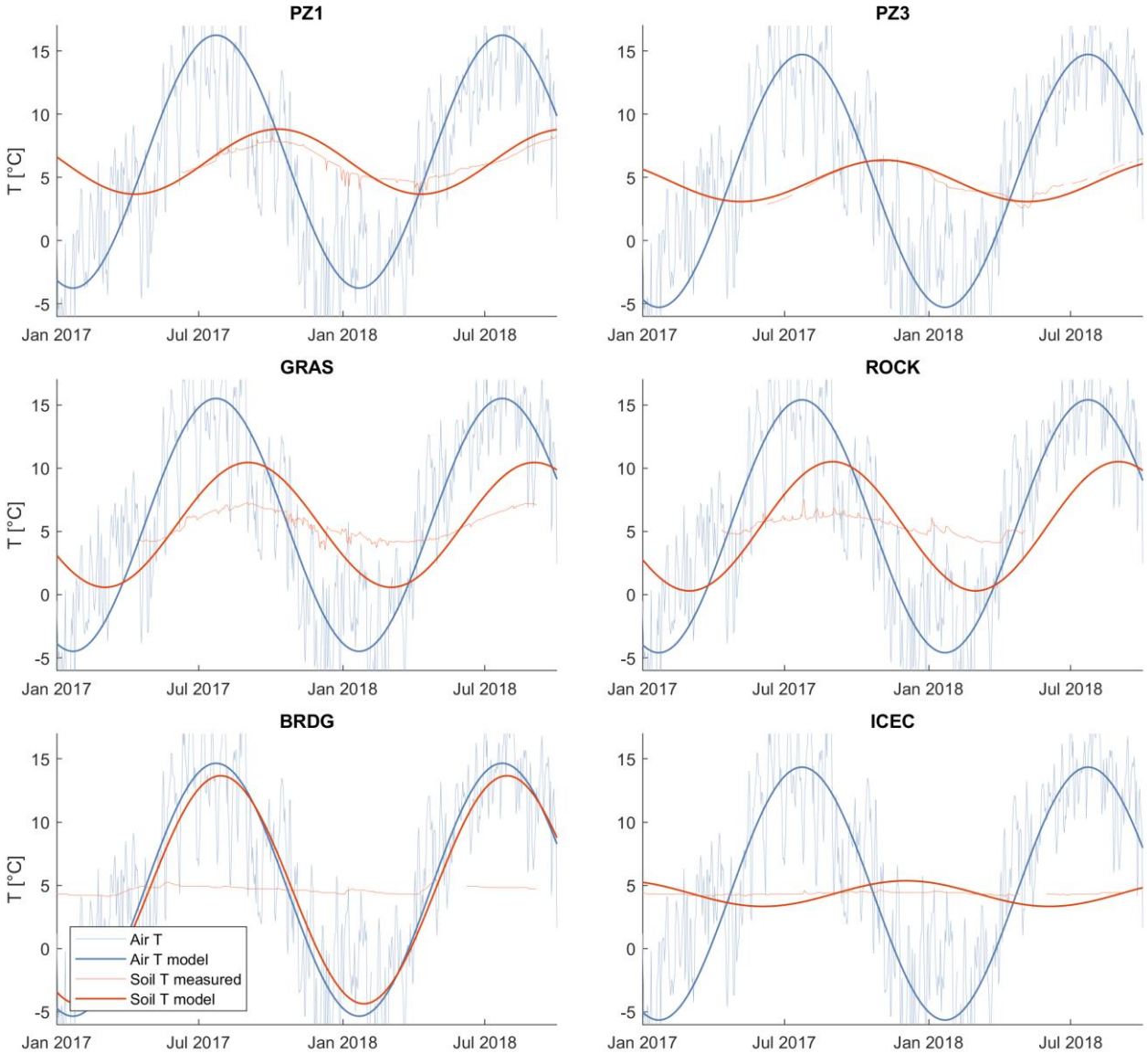

Figure 9. Measured and modelized air and soil temperature for 2 piezometers (PZ1 and PZ3) and 4 springs (GRAS, ROCK, BRDG and ICEC).

https://doi.org/10.5194/hess-2022-48
Preprint. Discussion started: 8 February 2022


Hydrology and Earth System Sciences
Discussions

775

Appendix 3: Lapse rate estimation

An isotopic lapse rate of 1.9 ‰/100/m for δ^2H and 0.27 ‰/100/m for $\delta^{18}O$ is calculated for Switzerland based on data from the Global Network of Isotopes in Precipitation (GNIP) between 1966 and 2014 (Beria et al., 2018). This lapse rate is twice
780 the lapse rate we compute from our precipitation water samples between the Auberge and Chalet stations: 0.84 ‰/100/m for δ^2H and 0.13 ‰/100/m for $\delta^{18}O$.

We make the hypothesis of a homogeneous rainfall input having such a lapse rate over the catchment (which is unrealistic regarding runoff, but conceivable at longer time scale, involving baseflow), and we estimate that a difference of isotopic composition of the streamflow water should appear between the two hydrological stations over the main river even for our
785 lower lapse rates. We focus on 2 periods for which we have a large number of stream water samples for both HyS1 and HyS2 (from November 5th, 2016 to December 7th, 2016 and June 13th, 2017 to November 15th, 2017).

The water collected by the whole catchment should be depleted by 0.87 ‰ in the heavy isotopes for δ^2H and 0.14 ‰ for $\delta^{18}O$. This difference is in the order of magnitude of the processing error (see section 3.6), and so should not be further commented following the stated hypothesis. The weak difference is due to the fact that the mean elevation is too close between the upper
790 subcatchment and the whole catchment, respectively 2196 m and 2165 masl

https://doi.org/10.5194/hess-2022-48
Preprint. Discussion started: 8 February 2022


Hydrology and Earth System Sciences
Discussions

References

Affolter, S., Hauselmann, A. D., Fleitmann, D., Hauselmann, P., and Leuenberger, M.: Triple isotope (delta D, delta O-17, delta O-18) study on precipitation, drip water and speleothem fluid inclusions for a Western Central European cave (NW Switzerland), Quaternary Sci Rev, 127, 73-89, DOI 10.1016/j.quascirev.2015.08.030, 2015.

Antoniazza, G., Nicollier, T., Boss, S., Mettra, F., Badoux, A., Schaefli, B., Rickenmann, D., and Lane, S.: Hydrological drivers of bedload transport in an Alpine watershed, Water Resources Research, https://www.essoar.org/doi/abs/10.1002/essoar.10507461.1, Submitted.

Arnoux, M., Brunner, P., Schaefli, B., Mott, R., Cochand, F., and Hunkeler, D.: Low-flow behavior of alpine catchments with varying quaternary cover under current and future climatic conditions, Journal of Hydrology, 125591, https://doi.org/10.1016/j.jhydrol.2020.125591, 2020.

Ba, R.: Origines et quantification de l 'eau utilisée par Larix decidua dans un bassin versant de haute montagne (Vallon de Nant – Suisse), Master Thesis, University of Lausanne, Switzerland, 50, 2019.

Badoux, H.: Aperçu géologique du Vallon de Nant. La Thomasia, Jardin alpin de Pont de Nant., Lausanne, 37-43, 1991.

Barkan, E., and Luz, B.: High precision measurements of O-17/O-16 and O-18/O-16 ratios in H2O, Rapid Commun Mass Sp, 19, 3737-3742, 10.1002/rcm.2250, 2005.

Benoit, L., Allard, D., and Mariethoz, G.: Stochastic Rainfall Modeling at Sub-kilometer Scale, Water Resources Research, 54, 4108-4130, 10.1029/2018WR022817, 2018.

Beria, H., Larsen, J. R., Ceperley, N. C., Michelon, A., Vennemann, T., and Schaefli, B.: Understanding snow hydrological processes through the lens of stable water isotopes, Wires Water, 5, 10.1002/wat2.1311, 2018.

Beria, H., Larsen, J. R., Michelon, A., Ceperley, N. C., and Schaefli, B.: HydroMix v1.0: a new Bayesian mixing framework for attributing uncertain hydrological sources, Geosci. Model Dev., 13, 2433-2450, 10.5194/gmd-13-2433-2020, 2020.

Beria, H., Benoit, L., Michelon, A., Mariéthoz, G., and Schaefli, B.: Improving hydrologic model realism by using stable water isotopes Hydrological Processes, In revision.

Bershaw, J., Hansen, D. D., and Schauer, A. J.: Deuterium excess and O-17-excess variability in meteoric water across the Pacific Northwest, USA, Tellus B, 72, 10.1080/16000889.2020.1773722, 2020.

Blahusiakova, A., Matouskova, M., Jenicek, M., Ledvinka, O., Kliment, Z., Podolinska, J., and Snopkova, Z.: Snow and climate trends and their impact on seasonal runoff and hydrological drought types in selected mountain catchments in Central Europe, Hydrol. Sci. J.-J. Sci. Hydrol., 65, 2083-2096, 10.1080/02626667.2020.1784900, 2020.

https://doi.org/10.5194/hess-2022-48
Preprint. Discussion started: 8 February 2022


Hydrology and Earth System Sciences
Discussions

Brauchli, T., Trujillo, E., Huwald, H., and Lehning, M.: Influence of Slope-Scale Snowmelt on Catchment Response Simulated With the Alpine3D Model, Water Resour Res, 53, 10723-10739, 10.1002/2017wr021278, 2017.

Brighenti, S., Tolotti, M., Bruno, M. C., Engel, M., Wharton, G., Cerasino, L., Mair, V., and Bertoldi, W.: After the peak water: the increasing influence of rock glaciers on alpine river systems, Hydrological Processes, 33, 2804-2823, 10.1002/hyp.13533, 2019.

Brunner, M. I., Farinotti, D., Zekollari, H., Huss, M., and Zappa, M.: Future shifts in extreme flow regimes in Alpine regions, Hydrol. Earth Syst. Sci., 23, 4471-4489, 10.5194/hess-23-4471-2019, 2019.

Cano-Paoli, K., Chiogna, G., and Bellin, A.: Convenient use of electrical conductivity measurements to investigate hydrological processes in Alpine headwaters, Sci. Total Environ., 685, 37-49, 10.1016/j.scitotenv.2019.05.166, 2019.

Ceperley, N., Michelon, A., Escoffier, N., Mayoraz, G., Boix Canadell, M., Horgby, A., Hammer, F., Antoniazza, G., Schaefli, B., Lane, S., Rickenmann, D., and Boss, S.: Salt gauging and stage-discharge curve, Avançon de Nant, outlet Vallon de Nant catchment, Zenodo, 10.5281/zenodo.1154798, 2018.

Ceperley, N., Zuecco, G., Beria, H., Carturan, L., Michelon, A., Penna, D., Larsen, J., and Schaefli, B.: Seasonal snow cover decreases young water fractions in high Alpine catchments, Hydrological Processes, 34, 4794-4813, https://doi.org/10.1002/hyp.13937, 2020.

Cherix, D., and Vittoz, P.: Synthèse et conclusions aux Journées de la biodiversité 2008 dans le Vallon de Nant, Biodiversité du Vallon de Nant, Mémoire de la Société vaudoise des Sciences naturelles, 23, 225-240, 2009.

Chiaudani, A., Di Curzio, D., and Rusi, S.: The snow and rainfall impact on the Verde spring behavior: A statistical approach on hydrodynamic and hydrochemical daily time-series, Sci. Total Environ., 689, 481-493, 10.1016/j.scitotenv.2019.06.433, 2019.

Cochand, M., Christe, P., Ornstein, P., and Hunkeler, D.: Groundwater Storage in High Alpine Catchments and Its Contribution to Streamflow, Water Resour Res, 55, 2613-2630, 10.1029/2018wr022989, 2019.

Constantz, J.: Heat as a tracer to determine streambed water exchanges, Water Resources Research, 44, https://doi.org/10.1029/2008WR006996, 2008.

Coplen, T. B.: Reporting of Stable Hydrogen, Carbon, and Oxygen Isotopic Abundances, Pure Appl Chem, 66, 273-276, DOI 10.1351/pac199466020273, 1994.

Dansgaard, W.: Stable Isotopes in Precipitation, Tellus, 16, 436-468, 1964.

Dutoit, A.: La Végétation de l'étage Subalpin Du Vallon de Nant, PhD Thesis, University of Lausanne, Switzerland, 131, 1983.

https://doi.org/10.5194/hess-2022-48
Preprint. Discussion started: 8 February 2022

Elias, E. A., Cichota, R., Torriani, H. H., and de Jong van Lier, Q.: Analytical soil-temperature model: correction for temporal variation of daily amplitude, Soil Science Society of America Journal, 68, 784-788, https://doi.org/10.2136/sssaj2004.7840, 2004.

Engel, M., Penna, D., Bertoldi, G., Dell'Agnese, A., Soulsby, C., and Comiti, F.: Identifying run-off contributions during melt-induced run-off events in a glacierized alpine catchment, Hydrological Processes, 30, 343-364, 10.1002/hyp.10577, 2016.

Floriancic, M. G., van Meerveld, I., Smoorenburg, M., Margreth, M., Naef, F., Kirchner, J. W., and Molnar, P.: Spatio-temporal variability in contributions to low flows in the high Alpine Poschiavino catchment, Hydrological Processes, 32, 3938-3953, doi:10.1002/hyp.13302, 2018.

Foster, L. M., Bearup, L. A., Molotch, N. P., Brooks, P. D., and Maxwell, R. M.: Energy budget increases reduce mean streamflow more than snow-rain transitions: using integrated modeling to isolate climate change impacts on Rocky Mountain hydrology, Environ. Res. Lett., 11, 10, 10.1088/1748-9326/11/4/044015, 2016.

Freudiger, D., Frielingsdorf, B., Stahl, K., Steinbrich, A., Weiler, M., Griessinger, N., and Seibert, J.: The Potential of meteorological gridded datasets for hydrological modeling in alpine basins, Hydrol Wasserbewirts, 60, 353-367, 10.5675/HyWa_2016,6_1, 2016.

Froehlich, K., Gibson, J. J., and Aggarwal, P. K.: Deuterium excess in precipitation and its climatological significance, International Atomic Energy Agency (IAEA) 2002.

Gallice, A., Schaefli, B., Lehning, M., Parlange, M. B., and Huwald, H.: Stream temperature prediction in ungauged basins: review of recent approaches and description of a new physics-derived statistical model, Hydrol Earth Syst Sc, 19, 3727-3753, 10.5194/hess-19-3727-2015, 2015.

Giaccone, E., Luoto, M., Vittoz, P., Guisan, A., Mariéthoz, G., and Lambiel, C.: Influence of microclimate and geomorphological factors on alpine vegetation in the Western Swiss Alps, Earth Surf Proc Land, 44, 3093– 3107, 10.1002/esp.4715, 2019.

Grand, S., Rubin, A., Verrecchia, E. P., and Vittoz, P.: Variation in Soil Respiration across Soil and Vegetation Types in an Alpine Valley, Plos One, 11, 10.1371/journal.pone.0163968, 2016.

Hammond, J. C., and Kampf, S. K.: Subannual Streamflow Responses to Rainfall and Snowmelt Inputs in Snow-Dominated Watersheds of the Western United States, Water Resour Res, 56, 10.1029/2019WR026132, 2020.

Hanus, S., Hrachowitz, M., Zekollari, H., Schoups, G., Vizcaino, M., and Kaitna, R.: Future changes in annual, seasonal and monthly runoff signatures in contrasting Alpine catchments in Austria, Hydrology and Earth System Sciences, 25, 3429-3453, 10.5194/hess-25-3429-2021, 2021.

Hayashi, M.: Alpine Hydrogeology: The Critical Role of Groundwater in Sourcing the Headwaters of the World, Groundwater, 58, 498-510, 10.1111/gwat.12965, 2020.

https://doi.org/10.5194/hess-2022-48
Preprint. Discussion started: 8 February 2022

Haynes, W. M., Lide, D. R., and Bruno, T. J.: CRC handbook of chemistry and physics, Boca Raton, Florida : CRC Press/Taylor & Francis, 2017.

He, Z. H., Tian, F. Q., Gupta, H. V., Hu, H. C., and Hu, H. P.: Diagnostic calibration of a hydrological model in a mountain area by hydrograph partitioning, Hydrology and Earth System Sciences, 19, 1807-1826, 2015.

Horgby, A., Canadell, M. B., Utseth, A. J., Vennemann, T. W., and Battin, T. J.: High-Resolution Spatial Sampling Identifies Groundwater as Driver of CO2 Dynamics in an Alpine Stream Network, J Geophys Res-Biogeo, 124, 1961-1976, 10.1029/2019jg005047, 2019.

Huggenberger, P.: Faltenmodelle und Verformungsverteilung in Deckenstrukturen am Beispiel der Morcles-Decke (Helvetikum der Westschweiz), Ph.D. Thesis, ETH-Zürich, Switzerland, 326, 10.3929/ethz-a-000365939, 1985.

Kane, D. L., Hinkel, K. M., Goering, D. J., Hinzman, L. D., and Outcalt, S. I.: Non-conductive heat transfer associated with frozen soils, Global Planet Change, 29, 275-292, Doi 10.1016/S0921-8181(01)00095-9, 2001.

Landais, A., Barkan, E., Yakir, D., and Luz, B.: The triple isotopic composition of oxygen in leaf water, Geochim Cosmochim Ac, 70, 4105-4115, 10.1016/j.gca.2006.06.1545, 2006.

Landais, A., Barkan, E., and Luz, B.: Record of delta O-18 and O-17-excess in ice from Vostok Antarctica during the last 150,000 years, Geophys Res Lett, 35, 10.1029/2007gl032096, 2008.

Landwehr, J. M., and Coplen, T. B.: Line-conditioned excess: a new method for characterizing stable hydrogen and oxygen isotope ratios in hydrologic systems, International Conference on Isotopes in Environmental Studies, Aquatic Forum, Monte-Carlo, Monaco, 25–29 October 2004, IAEA, Vienna, 132–135, 2006.

Lane, S. N., Borgeaud, L., and Vittoz, P.: Emergent geomorphic-vegetation interactions on a subalpine alluvial fan, Earth Surf Proc Land, 41, 72-86, 10.1002/esp.3833, 2016.

Leuenberger, M. C., and Ranjan, S.: Disentangle Kinetic From Equilibrium Fractionation Using Primary (delta O-17, delta O-18, delta D) and Secondary (Delta O-17, d(ex)) Stable Isotope Parameters on Samples From the Swiss Precipitation Network, Frontiers in Earth Science, 9, 10.3389/feart.2021.598061, 2021.

Linsbauer, A., Huss, M., Hodel, E., Bauder, A., Fischer, M., Weidmann, Y., Bärtschi, H., and Schmassmann, E.: The new Swiss Glacier Inventory SGI2016: From a topographical to a glaciological dataset, Frontiers in Earth Science, in review, 2021.

Livneh, B., and Badger, A. M.: Drought less predictable under declining future snowpack, Nature Climate Change, 10, 452-+, 10.1038/s41558-020-0754-8, 2020.

Lucianetti, G., Penna, D., Mastrorillo, L., and Mazza, R.: The Role of Snowmelt on the Spatio-Temporal Variability of Spring Recharge in a Dolomitic Mountain Group, Italian Alps, Water, 12, 26, 10.3390/w12082256, 2020.

https://doi.org/10.5194/hess-2022-48
Preprint. Discussion started: 8 February 2022

Mächler, E., Salyani, A., Walser, J. C., Larsen, A., Schaefli, B., Altermatt, F., and Ceperley, N.: Environmental DNA simultaneously informs hydrological and biodiversity characterization of an Alpine catchment, Hydrol. Earth Syst. Sci., 1-30, 10.5194/hess-25-735-2021, 2021.

Majoube, M.: Fractionnement en oxygène 18 et en deutérium entre l'eau et sa vapeur, J. Chim. Phys., 68, 1423-1436, 1971.

Meijer, H. A. J., and Li, W. J.: The use of electrolysis for accurate delta O-17 and delta O-18 isotope measurements in water, Isot Environ Healt S, 34, 349-369, Doi 10.1080/10256019808234072, 1998.

MeteoSwiss: Documentation of MeteoSwiss Grid-Data Products: Daily Precipitation (final analysis): RhiresD, 2019.

Michelon, A., Benoit, L., Beria, H., Ceperley, N., and Schaefli, B.: Benefits from high-density rain gauge observations for hydrological response analysis in a small alpine catchment, Hydrol. Earth Syst. Sci., 25, 2301-2325, 10.5194/hess-25-2301-2021, 2021a.

Michelon, A., Schaefli, B., Ceperley, N., and Beria, H.: Weather dataset from Vallon de Nant, Switzerland (from 16 August 2016 to 14 October 2018), Zenodo, https://doi.org/10.5281/zenodo.5518942, 2021b.

Muelchi, R., Rössler, O., Schwanbeck, J., Weingartner, R., and Martius, O.: Future runoff regime changes and their time of emergence for 93 catchments in Switzerland, Hydrol. Earth Syst. Sci. Discuss., 2020, 1-25, 10.5194/hess-2020-516, 2020.

Muelchi, R., Rossler, O., Schwanbeck, J., Weingartner, R., and Martius, O.: River runoff in Switzerland in a changing climate - runoff regime changes and their time of emergence, Hydrology and Earth System Sciences, 25, 3071-3086, 10.5194/hess-25-3071-2021, 2021.

Musselman, K. N., Addor, N., Vano, J. A., and Molotch, N. P.: Winter melt trends portend widespread declines in snow water resources, Nature Climate Change, 17, 10.1038/s41558-021-01014-9,

Nyamgerel, Y., Han, Y., Kim, M., Koh, D., and Lee, J.: Review on Applications of O-17 in Hydrological Cycle, Molecules, 26, 10.3390/molecules26154468, 2021.

Ochsner, T. E., Horton, R., and Ren, T. H.: A new perspective on soil thermal properties, Soil Science Society of America Journal, 65, 1641-1647, DOI 10.2136/sssaj2001.1641, 2001.

Ohlanders, N., Rodriguez, M., and McPhee, J.: Stable water isotope variation in a Central Andean watershed dominated by glacier and snowmelt, Hydrol. Earth Syst. Sci., 17, 1035-1050, 10.5194/hess-17-1035-2013, 2013.

Penna, D., Engel, M., Mao, L., Dell'Agnese, A., Bertoldi, G., and Comiti, F.: Tracer-based analysis of spatial and temporal variations of water sources in a glacierized catchment, Hydrol. Earth Syst. Sci., 18, 5271-5288, 10.5194/hess-18-5271-2014, 2014.

https://doi.org/10.5194/hess-2022-48
Preprint. Discussion started: 8 February 2022


Hydrology and Earth System Sciences
Discussions

Penna, D., van Meerveld, H. J., Zuecco, G., Fontana, G. D., and Borga, M.: Hydrological response of an Alpine catchment to rainfall and snowmelt events, Journal of Hydrology, 537, 382-397, 10.1016/j.jhydrol.2016.03.040, 2016.

Risi, C., Landais, A., Bony, S., Jouzel, J., Masson-Delmotte, V., and Vimeux, F.: Understanding the O-17 excess glacial-interglacial variations in Vostok precipitation, J Geophys Res-Atmos, 115, 10.1029/2008jd011535, 2010.

Rowley, M. C., Grand, S., and Verrecchia, E. P.: Calcium-mediated stabilisation of soil organic carbon, Biogeochemistry, 137, 27-49, 10.1007/s10533-017-0410-1, 2018.

Rucker, A., Zappa, M., Boss, S., and von Freyberg, J.: An optimized snowmelt lysimeter system for monitoring melt rates and collecting samples for stable water isotope analysis, J. Hydrol. Hydromech., 67, 20-31, 10.2478/johh-2018-0007, 2019.

Santos, A. C., Portela, M. M., Rinaldo, A., and Schaefli, B.: Analytical flow duration curves for summer streamflow in Switzerland, Hydrol Earth Syst Sc, 22, 2377-2389, 10.5194/hess-22-2377-2018, 2018.

Schaefli, B., Rinaldo, A., and Botter, G.: Analytic probability distributions for snow-dominated streamflow, Water Resour Res, 49, 1-13, 10.1002/2012WR020234, 2013.

Schaefli, B., Nicotina, L., Imfeld, C., Da Ronco, P., Bertuzzo, E., and Rinaldo, A.: SEHR-ECHO v1.0: a Spatially Explicit Hydrologic Response model for ecohydrologic applications, Geosci Model Dev, 7, 2733-2746, 10.5194/gmd-7-2733-2014, 2014.

Schaefli, B.: Snow hydrology signatures for model identification within a limits-of-acceptability approach, Hydrological Processes, 30, 4019-4035, 10.1002/hyp.10972, 2016.

Schaefli, B.: Average daily air temperature, precipitation and relative sunshine duration for Vallon de Nant catchment, extracted from gridded MeteoSwiss data (1961-2020), Zenodo, https://doi.org/10.5281/zenodo.5420415, 2021.

Schauer, A. J., Schoenemann, S. W., and Steig, E. J.: Routine high-precision analysis of triple water-isotope ratios using cavity ring-down spectroscopy, Rapid Commun Mass Sp, 30, 2059-2069, 10.1002/rcm.7682, 2016.

Schotterer, U., Stichler, W., and Ginot, P.: The Influence of Post-Depositional Effects on Ice Core Studies: Examples From the Alps, Andes, and Altai, Springer Netherlands 2004.

Schurch, M., Kozel, R., Schotterer, U., and Tripet, J. P.: Observation of isotopes in the water cycle - the Swiss National Network (NISOT), Environ Geol, 45, 1-11, 10.1007/s00254-003-0843-9, 2003.

Sprenger, M., Leistert, H., Gimbel, K., and Weiler, M.: Illuminating hydrological processes at the soil-vegetation-atmosphere interface with water stable isotopes, Reviews of Geophysics, 54, 2015RG000515, 10.1002/2015RG000515, 2016.

Surma, J., Assonov, S., and Staubwasser, M.: Triple Oxygen Isotope Systematics in the Hydrologic Cycle,, Reviews in Mineralogy and Geochemistry, 401–428, https://doi.org/10.2138/rmg.2021.86.12, 2021.

https://doi.org/10.5194/hess-2022-48
Preprint. Discussion started: 8 February 2022


Hydrology and Earth System Sciences
Discussions

swissAlti3D: The digital elevation model of Switzerland, 2012.

The MathWorks, I.: Curve Fitting Toolbox, https://www.mathworks.com/products/curvefitting.html, 2017.

Thornton, J. M.: Fully-integrated hydrological modelling in steep, snow-dominated, geologically complex Alpine terrain, PhD Thesis, University of Neuchâtel, Switzerland, 2021.

Thornton, J. M., Brauchli, T., Mariethoz, G., and Brunner, P.: Efficient multi-objective calibration and uncertainty analysis of distributed snow simulations in rugged alpine terrain, Journal of Hydrology, 126241, https://doi.org/10.1016/j.jhydrol.2021.126241, 2021a.

Thornton, J. M., Therrien, R., Mariéthoz, G., Linde, N., and Brunner, P.: Simulating fully-integrated hydrological dynamics in complex Alpine headwaters, EarthArXiv, pre-print, doi.org/10.31223/X5RG7Q, 2021b.

Trask, J. C., Devine, S. M., and Fogg, G. E.: Soil temperature survey in a mountain basin, Geoderma, 367, 114202, https://doi.org/10.1016/j.geoderma.2020.114202, 2020.

Vittoz, P.: Permanent.Plot.ch – a database for Swiss permanent vegetation plots, Biodiversity & Ecology, 4, 337-337, 2012.

Vittoz, P.: Soil temperature series in Vallon de Nant catchment, Switzerland, Zenodo, http://doi.org/10.5281/zenodo.4715669, 2021.

von Freyberg, J., Knapp, J. L. A., Rücker, A., Studer, B., and Kirchner, J. W.: Technical note: Evaluation of a low-cost evaporation protection method for portable water samplers, Hydrol. Earth Syst. Sci., 24, 5821-5834, 10.5194/hess-24-5821-2020, 2020.

Webb, R. W., Wigmore, O., Jennings, K., Fend, M., and Molotch, N. P.: Hydrologic connectivity at the hillslope scale through intra-snowpack flow paths during snowmelt, Hydrological Processes, 34, 1616-1629, 10.1002/hyp.13686, 2020.

Wei, Z. W., Lee, X., Aemisegger, F., Benetti, M., Berkelhammer, M., Casado, M., Caylor, K., Christner, E., Dyroff, C., Garcia, O., Gonzalez, Y., Griffis, T., Kurita, N., Liang, J., Liang, M. C., Lin, G. H., Noone, D., Gribanov, K., Munksgaard, N. C., Schneider, M., Ritter, F., Steen-Larsen, H. C., Vallet-Coulomb, C., Wen, X. F., Wright, J. S., Xiao, W., and Yoshimura, K.: A global database of water vapor isotopes measured with high temporal resolution infrared laser spectroscopy, Sci Data, 6, 10.1038/sdata.2018.302, 2019.

Zuecco, G., Carturan, L., De Blasi, F., Seppi, R., Zanoner, T., Penna, D., Borga, M., Carton, A., and Dalla Fontana, G.: Understanding hydrological processes in glacierized catchments: Evidence and implications of highly variable isotopic and electrical conductivity data, Hydrological Processes, 33, 816-832, 10.1002/hyp.13366, 2019.